universe

MDPI

Review

Latest Results from RHIC + Progress on Determining $\hat{q}L$ in RHI Collisions Using Di-Hadron Correlations

Michael J. Tannenbaum

Physics Department, Brookhaven National Laboratory, Upton, NY 11973-5000, USA; mjt@bnl.gov

Received: 15 April 2019; Accepted: 24 May 2019; Published: 5 June 2019

Abstract: Results from Relativistic Heavy Ion Collider Physics in 2018 and plans for the future at Brookhaven National Laboratory are presented.

Keywords: RHIC qhat dihadron correlations

1. Introduction

The Relativistic Heavy Ion Collider (RHIC) at Brookhaven National Laboratory (BNL) is one of the two remaining operating hadron colliders in the world, and the first and only polarized p+p collider. BNL is located in the center of the roughly 200 km long maximum 40 km wide island (named Long Island), and appears on the map as the white circle which is the berm containing the Relativistic Heavy Ion Collider (RHIC). BNL is 100 km from New York City in a region which nurtures science with Columbia University and the Bronx High School of Science indicated (Figure 1). Perhaps more convincing is the list of the many Nobel Prize winners from New York City High School graduates (Figure 2) which does not yet include one of this years Nobel Prize winners in Physics, Arthur Ashkin who graduated from James Madison High school in 1940 and Columbia U. in 1947.

Figure 1. NASA infra-red photo of Long Island and the New York Metro Region from space. RHIC is the white circle to the left of the word BNL. Manhattan Island in New York City, ∼100 km west of BNL, is also clearly visible on the left side of the photo, with Columbia U. and Bronx Science High School indicated.

Number of laureates by secondary school		Class	Name of laureate	Award and year		University
8	The Bronx High School of Science, Bronx, New York City, NY	1947	Leon N. Cooper[1]	Physics	1972	Brown University
		1950	Sheldon Glashow[1][2]	Physics	1979	Columbia University
		1950	Steven Weinberg[1]	Physics	1979	Cornell University
		1949	Melvin Schwartz[1][3]	Physics	1988	Columbia University
		1966	Russell Hulse[1][4]	Physics	1993	Princeton University
		1966	H. David Politzer[1]	Physics	2004	California Institute of Technology
		1941	Roy Glauber[1][5]	Physics	2005	Harvard University
		1959	Robert Lefkowitz[6]	Chemistry	2012	Columbia University
4	James Madison High School, Brooklyn, New York City, NY	1939	Stanley Cohen[15]	Medicine	1986	Vanderbilt University
		1940	Robert Solow[16]	Economics	1987	Massachusetts Institute of Technology
		1943	Martin Lewis Perl[17]	Physics	1995	University of Michigan
		1947	Gary Becker[18]	Economics	1992	University of Chicago
4	Stuyvesant High School, Manhattan, New York City, NY	1941	Joshua Lederberg[19][20]	Medicine	1958	Rockefeller University
		1954	Roald Hoffmann[20][21]	Chemistry	1981	Cornell University
		1944	Robert Fogel[20][22]	Economics	1993	Cornell University
		1963	Richard Axel[20][23]	Medicine	2004	Columbia University
3	Abraham Lincoln High School, Brooklyn, New York City, NY	1933	Arthur Kornberg[31]	Medicine	1959	Stanford University
		1943	Paul Berg[31]	Chemistry	1980	Stanford University
		1933	Jerome Karle[31][32]	Chemistry	1985	City College of New York
3	Far Rockaway High School, Queens, New York City, NY	1935	Richard Feynman[33][34]	Physics	1965	California Institute of Technology
		1948	Burton Richter[34][35]	Physics	1976	Stanford University
		1942	Baruch Blumberg[34]	Medicine	1976	University of Pennsylvania
3	Townsend Harris High School, Queens, New York City, NY originally Manhattan, New York City, NY	1933	Herbert A. Hauptman[45]	Chemistry	1985	City College of New York
		1933	Julian Schwinger[45]	Physics	1965	Harvard University
		1936	Kenneth Arrow[45]	Economics	1972	City College of New York
2	Brooklyn Technical High School, Brooklyn, New York City, NY	1954	Arno Penzias	Physics	1978	City College of New York
		1922	George Wald	Biology	1987	Harvard University
2	Erasmus Hall High School, Brooklyn, New York City, NY	1919	Barbara McClintock[52]	Medicine or Physiology	1983	Cold Spring Harbor Laboratory
		1944	Eric Kandel[53]	Medicine or Physiology	2000	Columbia University
2	Hastings High School (New York)	1951	Edmund S. Phelps	Economics	2006	Columbia University
	Hastings High School (New York)	1962	Robert C. Merton	Economics	1997	MIT Sloan School of Management
2	Martin Van Buren High School, Queens, New York	1967	Frank Wilczek[57]	Physics	2004	University of Chicago Princeton University
		1967	Alvin Roth[58]	Economics	2012	Columbia University Stanford University
2	Walton High School, Bronx, New York City, NY	1941	Rosalyn Sussman Yalow[45]	Medicine and Physiology	1977	Hunter College
		1933	Gertrude B. Elion[45]	Medicine and Physiology	1988	Duke University
1	Manual Training HS, Brooklyn NY	1916	Issidor Isaac Rabi	Physics	1944	Columbia University
1	DeWitt Clinton HS, Bronx, NY	1931	Robert Hofstadter	Physics	1961	Stanford University
1	James Monroe High School, Bronx NY	1939	Leon Max Lederman	Physics	1988	Columbia University
1	New Trier High School, Winnetka, Illinois	1938	Jack Steinberger[90]	Physics	1988	Columbia University
1	Regis High School, Manhattan, New York City, NY	1957	John O'Keefe	Medicine	2014	City College of New York McGill University

Figure 2. From Wikipedia (edited), Physicists in blue and Roald Hoffman a classmate of mine from Columbia.

There also have been many discoveries and Nobel Prizes at BNL (Figure 3).

In particular, Leon Lederman, who made many discoveries at BNL (Figure 4), died this year (2018) at the age of 96. Leon was the most creative and productive high energy physics experimentalist of his generation as well as the physicist with the best jokes. He was also my PhD thesis Professor. For more details, see https://physicstoday.scitation.org/do/10.1063/PT.6.4.20181010a/full/.

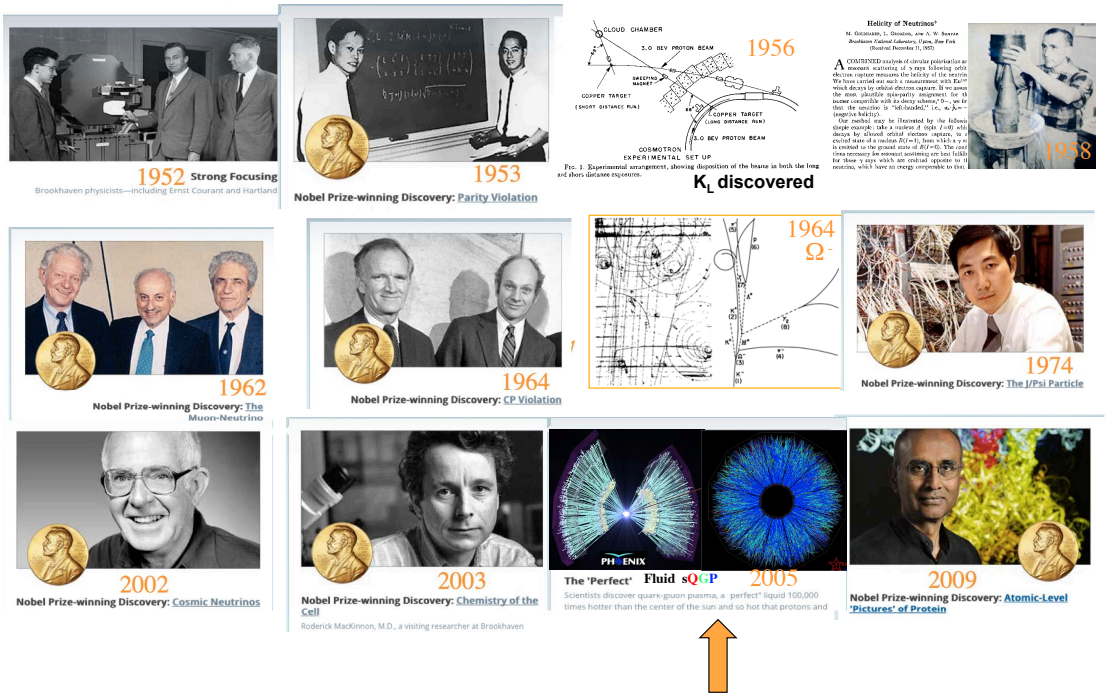

Figure 3. Selected Discoveries and Nobel Prizes at BNL, arrow points to QGPdiscovery.

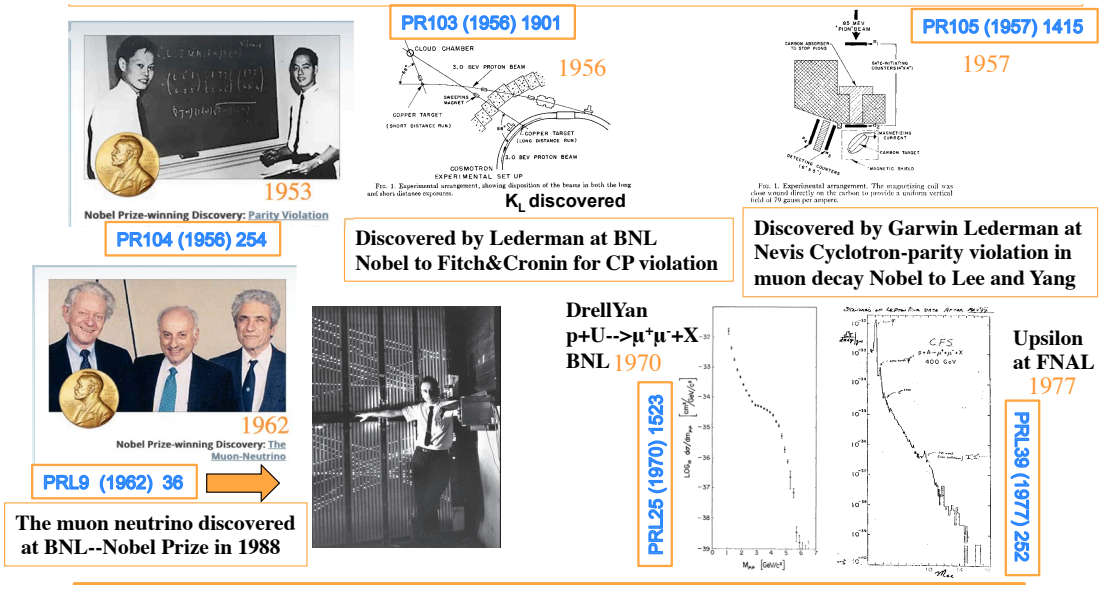

Figure 4. Discoveries by Leon Lederman and close associates at Columbia University.

2. Why RHIC Was Built: To Discover the Quark Gluon Plasma (QGP)

Figure 5 shows central collision particle production in the PHENIX and STAR detectors, which were the major detectors at RHIC.

At the startup of RHIC in the year 2000, there were two smaller more special purpose detectors PHOBOS and BRAHMS, as shown in Figure 6, which finished data taking in 2005.

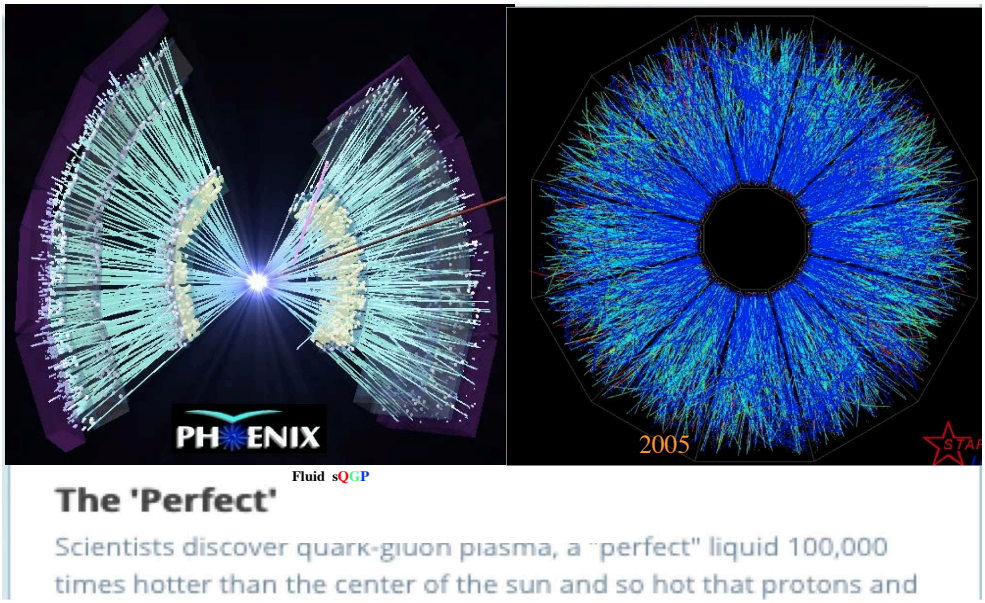

Figure 5. View along the beam direction of tracks of charged particles from central collision events in Au+Au collisions in the PHENIX and STAR detectors at RHIC.

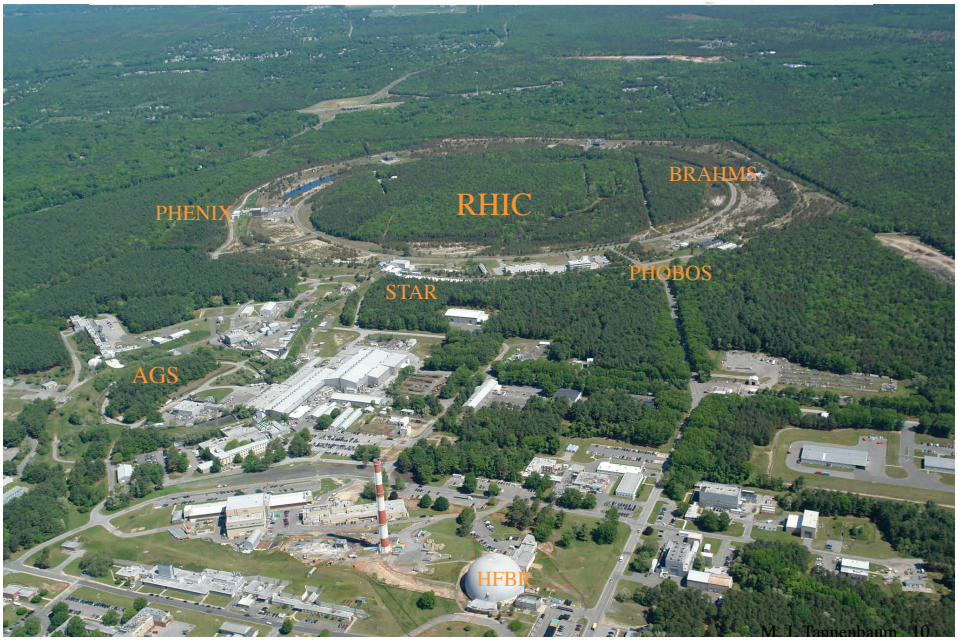

Figure 6. View of RHIC location from the air. The positions of the four original detectors, PHENIX, STAR PHOBOS and BRAHMS are indicated as well as the AGS (with three Nobel Prizes shown in Figure 3).

2.1. The First Major RHIC Experiments

The two major experiments at RHIC were STAR (Figure 7), which is still operating, and PHENIX (Figure 8), which finished data taking at the end of the 2016 run.

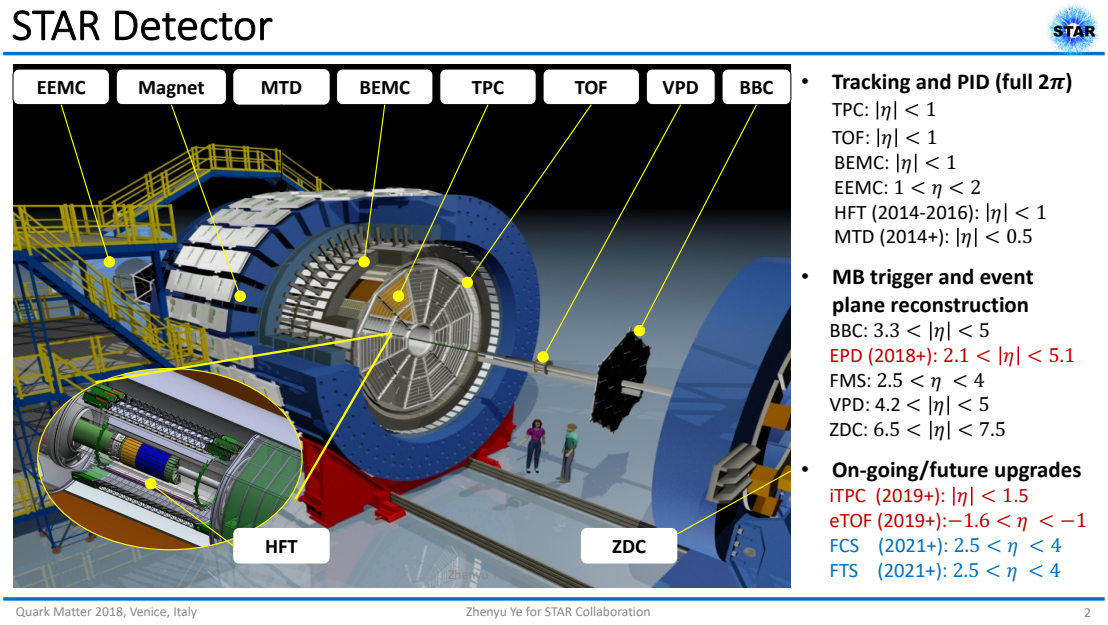

Figure 7. STAR is based on a normal conductor solenoid with Time Projection Chamber for tracking, an EM Calorimeter, Vertex detector and μ detector behind the thick iron yoke.

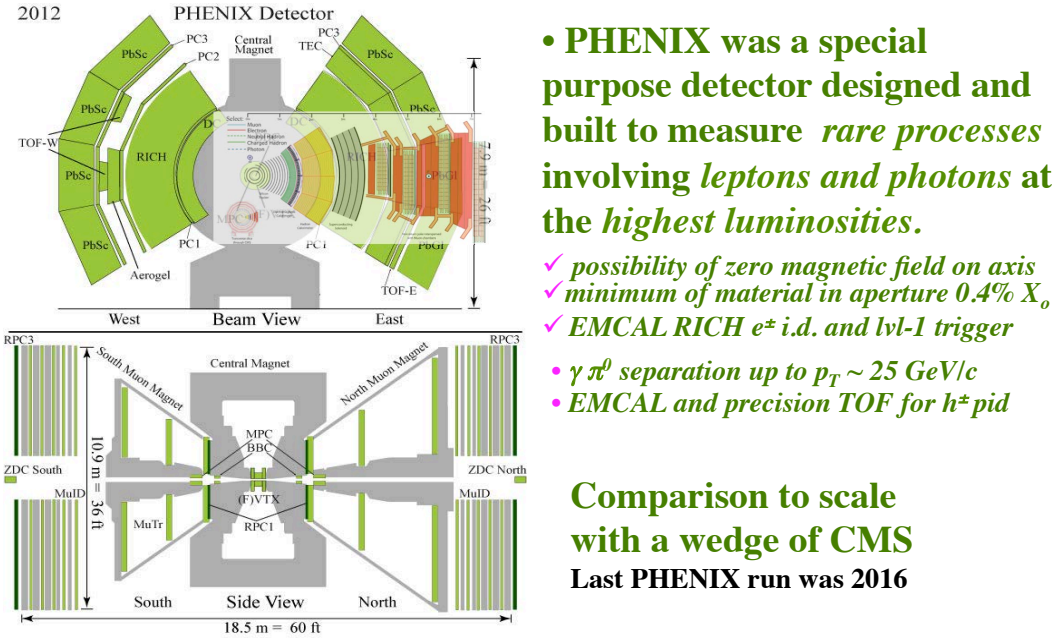

Figure 8. As indicated on the figure, PHENIX is a special purpose detector for electrons and photons but also measures charged hadrons and notably $\pi^0 \rightarrow \gamma + \gamma$ at mid-rapidity and muons in the forward direction.

2.2. The New Major RHIC Experiment sPHENIX

sPHENIX is a major improvement over PHENIX with a superconducting thin coil solenoid which was surplus from the BABAR experiment at SLAC and is now working at BNL and has reached its full field (Figure 9).

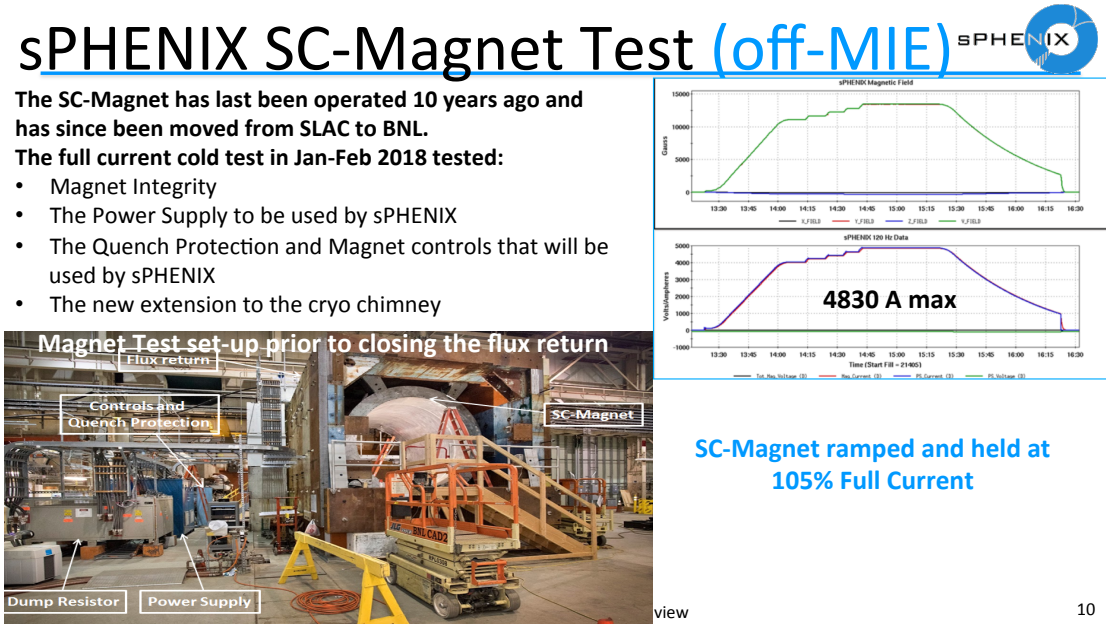

Figure 9. BABAR superconducting solenoid now in operation at BNL.

The design of the sPHENIX experiment is moving along well (Figure 10) with a notable addition of a hadron calorimeter based on the iron return yoke of the solenoid.

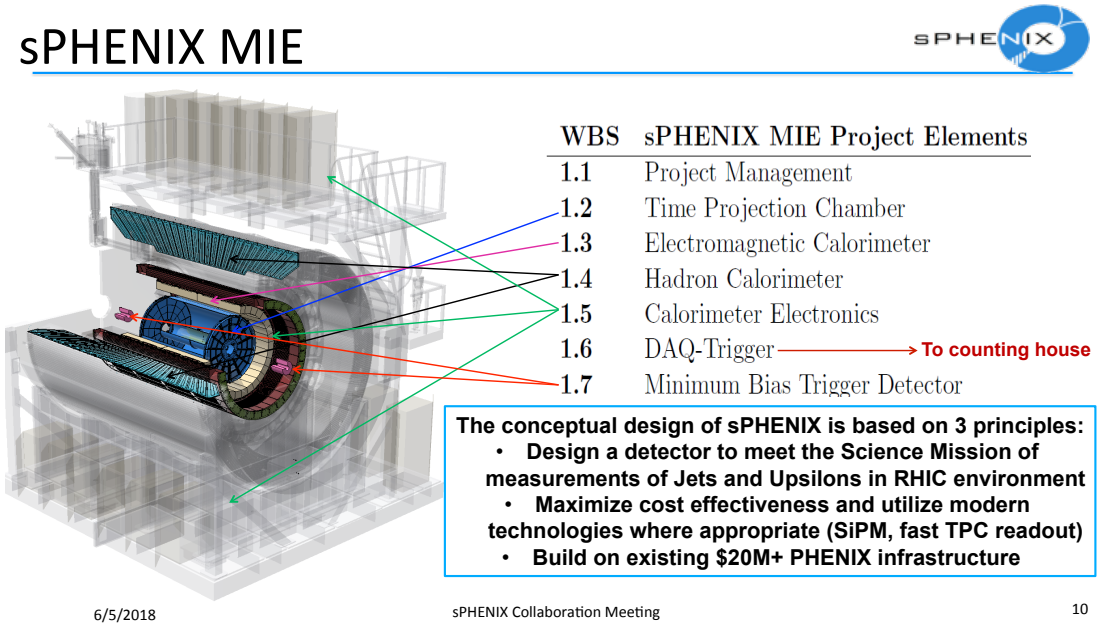

Figure 10. Conceptual design of sPHENIX with major features illustrated.

sPHENIX has been approved by the U. S. Department of Energy (DoE) as a Major Item of Equipment (MIE) with the schedule of critical decisions shown in Figure 11a, and the planned multi-year RHIC runs indicated in Figure 11b. The present sPHENIX collaboration and its evolution is shown in Figure 12.

Critical Decision Level 1 MIE Schedule

U.S. DEPARTMENT OF ENERGY
Office of Science

Milestone	Schedule Date
CD-0, Approve Mission Need	9/27/2016
CD-1/3A, Approve Alternative Selection and Cost Range. Long Lead Procurements	Q4 FY 2018
CD-2/3, Approve Performance Baseline	Q4 FY 2019
CD-4, Approve Project Completion	Q1 FY 2023

a)

Multi-year run plan for sPHENIX

sPHENIX

Year	Species	Energy [GeV]	Phys. Wks	Rec. Lum.	Samp. Lum.	Samp. Lum. All-Z
Year-1	Au+Au	200	16.0	7 nb^{-1}	8.7 nb^{-1}	34 nb^{-1}
Year-2	p+p	200	11.5	—	48 pb^{-1}	267 pb^{-1}
Year-2	p+Au	200	11.5	—	0.33 pb^{-1}	1.46 pb^{-1}
Year-3	Au+Au	200	23.5	14 nb^{-1}	26 nb^{-1}	88 nb^{-1}
Year-4	p+p	200	23.5	—	149 pb^{-1}	783 pb^{-1}
Year-5	Au+Au	200	23.5	14 nb^{-1}	48 nb^{-1}	92 nb^{-1}

b)

Figure 11. (**a**) DoE Critical Decision Schedule; and (**b**) multi-year run plan for sPHENIX.

sPHENIX collaboration evolution

sPHENIX

Augustana University
Banaras Hindu University
Baruch College, CUNY
Brookhaven National Laboratory
CEA Saclay
Central China Normal University
Chonbuk National University
Columbia University
Eötvös University
Florida State University
Georgia State University
Howard University
Hungarian sPHENIX Consortium
Insititut de physique nucléaire d'Orsay
Institute for High Energy Physics, Protvino
Institute of Nuclear Research, Russian Academy of Sciences, Moscow
Institute of Physics, University of Tsukuba
Iowa State University
Japan Atomic Energy Agency
Joint Czech Group
Korea University
Lawrence Berkeley National Laboratory
Lawrence Livermore National Laboratory
Lehigh University
Los Alamos National Laboratory
Massachusetts Institute of Technology
Muhlenberg College
Nara Women's University
National Research Centre "Kurchatov Institute"
National Research Nuclear University "MEPhI"
New Mexico State University
Oak Ridge National Laboratory
Ohio University
Petersburg Nuclear Physics Institute
Purdue University
Rice University
RIKEN
RIKEN BNL Research Center
Rikkyo University
Rutgers University
Saint-Petersburg Polytechnic University
Stony Brook University
Temple University
Tokyo Institute of Technology
Universidad Técnica Federico Santa María
University of California, Berkeley
University of California, Los Angeles
University of California, Riverside
University of Colorado, Boulder
University of Debrecen
University of Houston
University of Illinois, Urbana-Champaign
University of Jammu
University of Maryland
University of Michigan
University of New Mexico
University of Tennessee, Knoxville
University of Texas, Austin
University of Tokyo
Vanderbilt University
Wayne State University
Weizmann Institute
Yale University
Yonsei University

Next meeting: BNL, June '18

Santa Fe, Dec '17

BNL, June '17

GSU (Atlanta), Dec '16

BNL, June '16

Rutgers, Dec'15

May 23-25, 2018 sPHENIX DOE-OPA CD-1/3A Review

Figure 12. List of the sPHENIX collaboration members in June 2018 together with photos showing the evolution since December 2015. Dave Morrison (BNL) and Gunther Roland (MIT) are spokespersons.

2.3. Following RHIC in U.S. Nuclear Physics: the Electron Ion Collider (EIC)

Statement by Brookhaven Lab, Jefferson Lab, and the Electron-Ion Collider Users Community on National Academy of Sciences Electron-Ion Collider (EIC) Report

July 24, 2018

On July 24, 2018, a National Academy of Sciences (NAS) committee issued a report of its findings and conclusions related to the science case for a future U.S.-based Electron-Ion Collider (EIC) and the opportunities it would offer the worldwide nuclear physics community.

The committee's report—commissioned by the U.S. Department of Energy (DOE)—comes after 14 months of deliberation and meetings held across the U.S. to gather input from the nuclear science community. The report's conclusions include the following:

- The committee concludes that the science questions regarding the building blocks of matter are compelling and that an EIC is essential to answering these questions.
- The answers to these fundamental questions about the nature of the atoms will also have implications for particle physics and astrophysics and possibly other fields.
- Because an EIC will require significant advances and innovations in accelerator technologies, the impact of constructing an EIC will affect all accelerator-based sciences.
- In summary, the committee concludes that an EIC is timely and has the support of the nuclear science community. The science that it will achieve is unique and world leading and will ensure global U.S. leadership in nuclear science as well as in the accelerator science and technology of colliders.

The first BNL EIC design in 2014 is shown in Figure 13. The 2018 JLab and BNL EIC designs are shown in Figures 14 and 15.

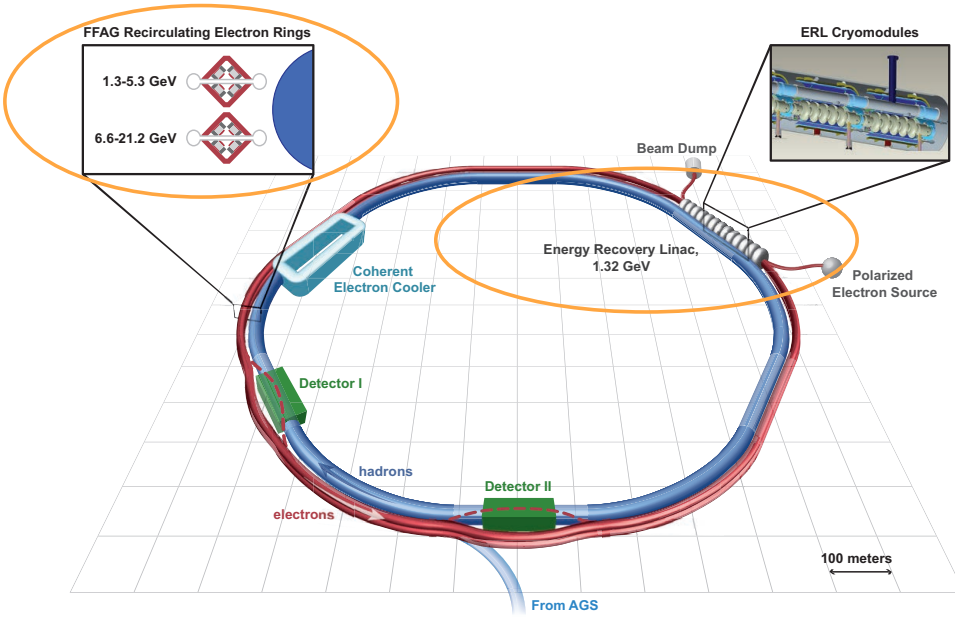

Figure 13. The 2014 cost estimate: BNL $755.9M; Temple NSAC subcommittee cost estimate $1.5B.

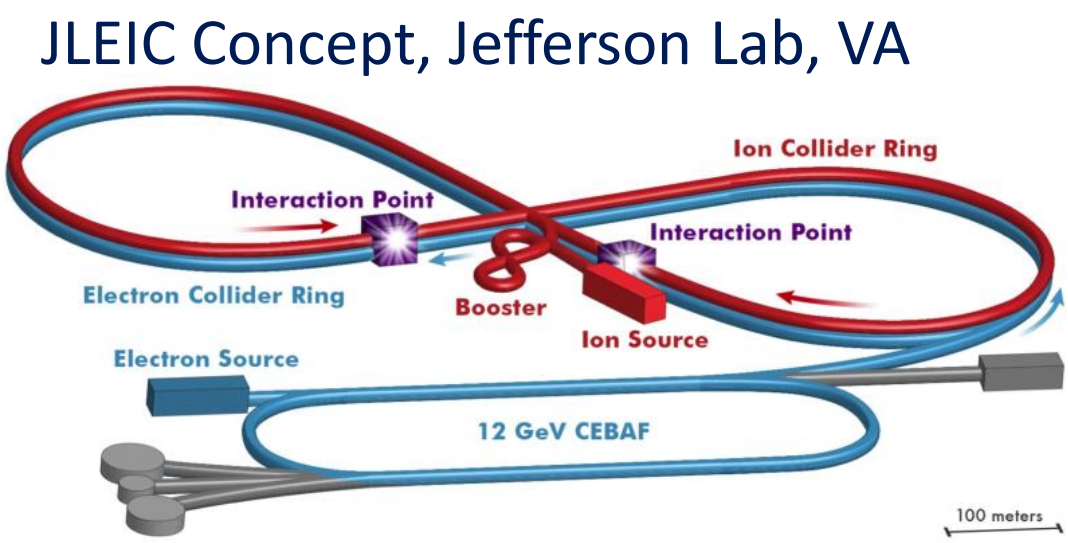

Figure 14. JLab EIC Concept. Temple committee cost estimate also $1.5B but no new accelerator technology required.

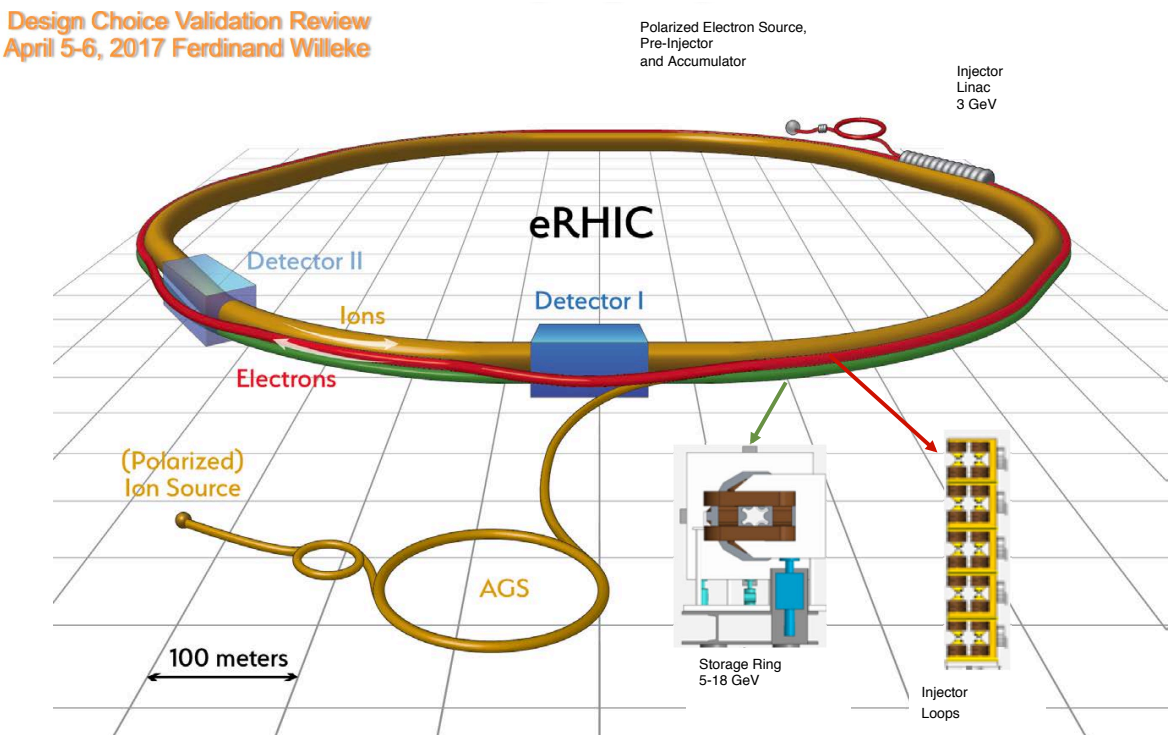

Figure 15. BNL eRHIC design progress 2017. Temple committee cost estimate $1.5B.

The two new designs of the JLab (JLEIC) and BNL (eRHIC) both satisfy the Temple committee cost estimate of $1.5B, but R&D of the novel first BNL design is not idle.

Research and Development (R&D) for an Improved Less Expensive BNL Machine Is Ongoing

BNL and Cornell are in the process of experiments studying an energy recovery linac ERL (Figure 16a). Figure 16b is the main Linac cryo module made from superconducting RF cavities. Figure 16c is a return loop made from fixed-field alternating-gradient (FFAG) optics made with permanent Halbach magnets to contain four beam energies in a single 70 mm-wide beam pipe, designed and prototyped at Brookhaven National Laboratory (BNL).

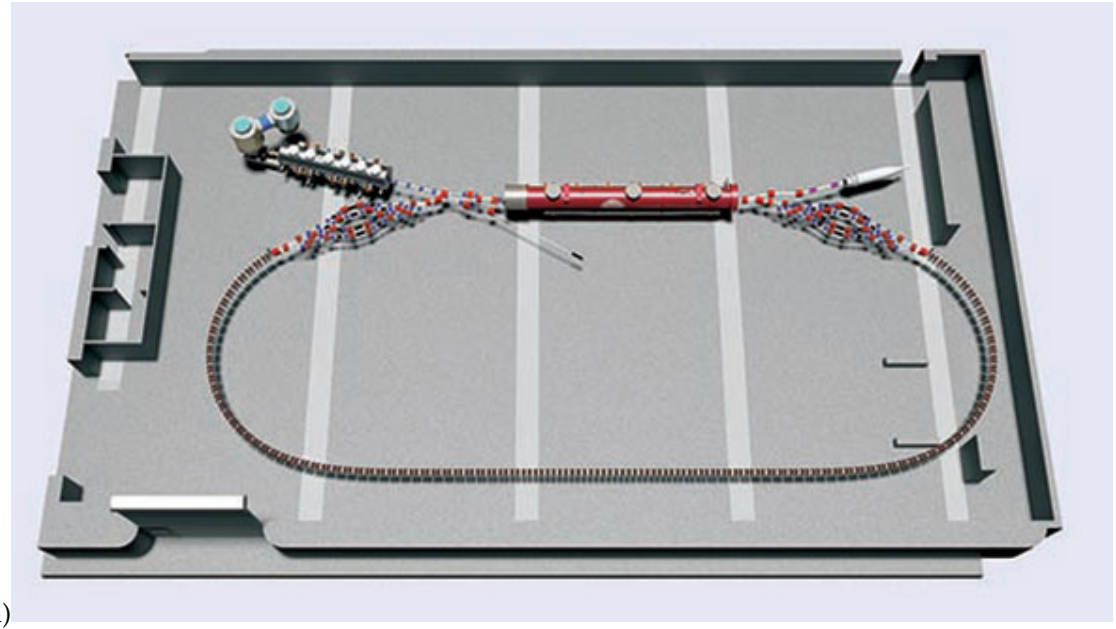

a)

Small Accelerator Promises Big Returns

Under construction in the US, the CBETA multi-turn energy-recovery linac will pave the way for accelerators that combine the best of linear and circular machines

March 16, 2018

b) The main linac cryomodule.

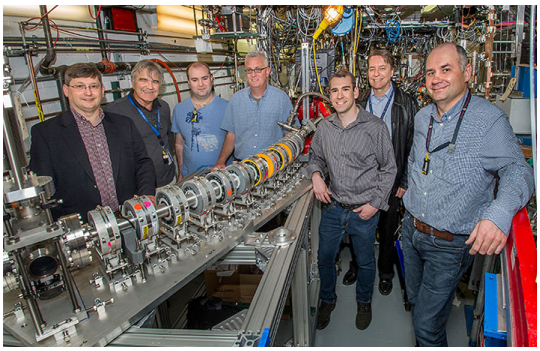

c) Members of the team testing a fixed-field, alternating-gradient beam transport line made with permanent magnets at Brookhaven Lab's Accelerator Test Facility (ATF), left to right: Mark Palmer (Director of ATF), Dejan Trbojevic, Stephen Brooks, George Mahler, Steven Trabocchi, Thomas Roser, and Mikhail Fedurin (ATF operator and experimental liaison).

Figure 16. (**a**) CBETA (Cornell-Brookhaven Energy Recovery Linac (ERL)); (**b**) Main Linac cryo module; and (**c**) FFAG permanent loop return loop.

3. RHIC Future Run Plan (Figure 17) and and the Present RHIC Run in 2018 (Figure 18)

3.1. 2018 RHIC Run Is $_{40}Zr^{96}$ + $_{40}Zr^{96}$ *and* $_{44}Ru^{96}$ + $_{44}Ru^{96}$*, Why?*

To determine whether the separation of charges in the flow, v_2, of π^+ and π^- shown in Figure 19 is due to a new phenomenon called the Chiral Magnetic Effect (Figure 20a), the 2018 measurements are made with collisions of Zr+Zr and Ru+Ru, which have the same number of nucleons but different electric charges (Figure 20b). If the effect is larger in Ru+Ru with stronger charge and magnetic field compared to Zr+Zr with the same number of nucleons, it would indicate that the charge asymmetry is a magnetic effect, possibly the Chiral Magnetic Effect.

BNL's future plan 2017 still works in 2018

Years	Beam Species and	Science Goals	New Systems
2014	Au+Au at 15 GeV Au+Au at 200 GeV ^{3}He+Au at 200 GeV	Heavy flavor flow, energy loss, thermalization, etc. Quarkonium studies QCD critical point search	Electron lenses 56 MHz SRF STAR HFT STAR MTD
2015-16	p↑+p↑ at 200 GeV p↑+Au, p↑+Al at 200 GeV High statistics Au+Au ~~Au+Au at 62 GeV ?~~ d+Au @ 200, 62, 39, 20 GeV	Extract η/s(T) + constrain initial quantum fluctuations Complete heavy flavor studies Sphaleron tests Parton saturation tests	PHENIX MPC-EX STAR FMS preshower Roman Pots Coherent e-cooling test
2017	p↑+p↑ at 510 GeV	Transverse spin physics Sign change in Sivers function	Coherent e-cooling final
2018	~~No Run~~ isobars	96Zr+96Zr and 96Ru+96Ru to test chiral magnetic effect on observed Au+Au charge separation effects	Low energy e-cooling install. STAR iTPC upgrade
2019-20	Au+Au at 5-20 GeV (BES-2)	Search for QCD critical point and onset of deconfinement	Low energy e-cooling
2022-23 ~~2021-22~~	Au+Au at 200 GeV p↑+p↑, p↑+Au at 200 GeV	Jet, di-jet, γ-jet probes of parton transport and energy loss mechanism Color screening for different quarkonia Forward spin & initial state physics	sPHENIX Forward upgrades ?
2024-26 ≥ 2023 ?	Factor of 10 increase Au+Au ~~No Runs~~ Factor of 4 increase p+p	Complete above measurements	Transition to eRHIC

This color is sPHENIX proposed run plan

Figure 17. RHIC run plan 2014–2023 (2026?).

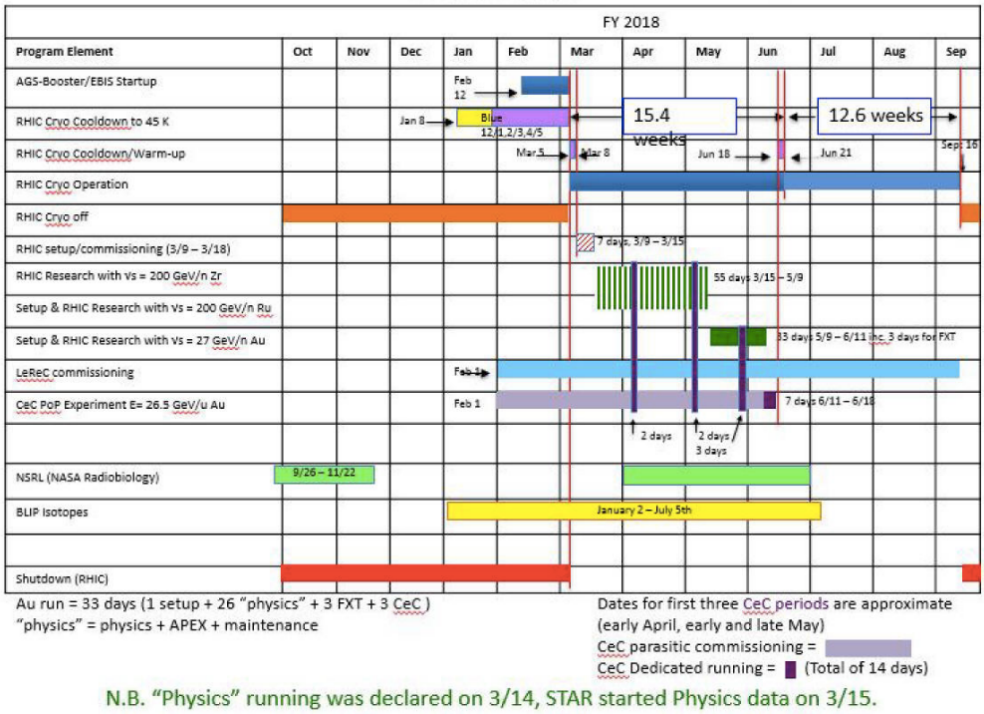

Figure 18. The 2018 RHIC run schedule.

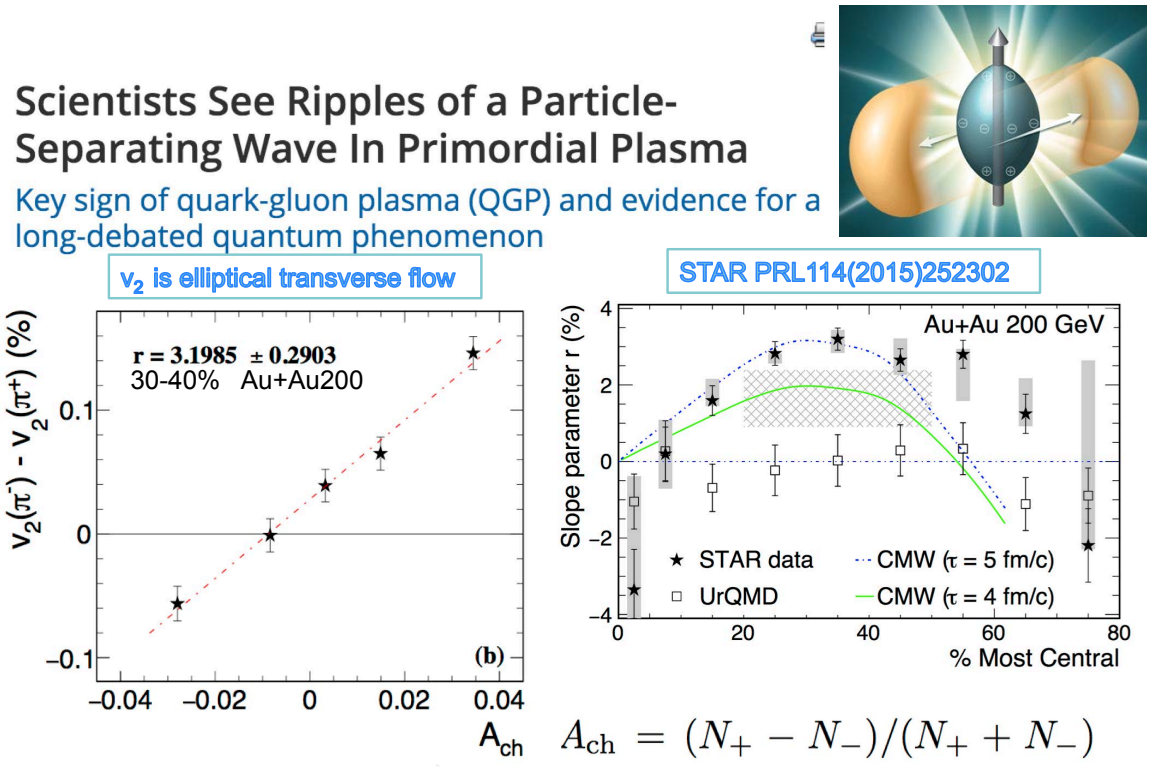

Figure 19. From Article in the BNL news 8 June 2015.

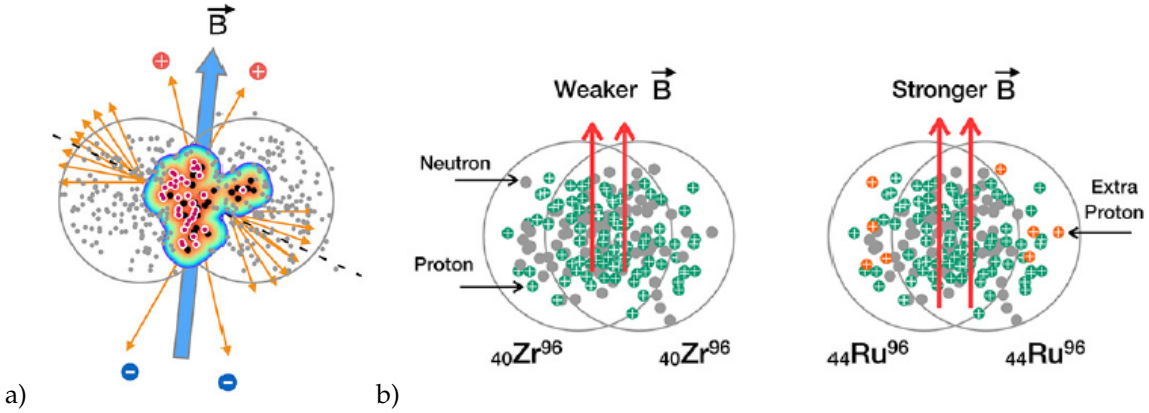

Figure 20. (**a**) Schematic of A+A collision; and (**b**) sketch of the stronger magnetic (B) field in Ru+Ru.

3.2. Vorticity: An Application of Particle Physics to the QGP

It was observed at FERMILAB [1] that forward Λ were polarized in p+Be collisions, where the proton in the $\Lambda \rightarrow p + \pi^-$ decay is emitted along the spin direction of the Λ. In the A+A collision (Figure 21a), the forward going beam fragments are deflected outwards so that the event plane and the angular momentum $\hat{J}_{sys}$ of the QGP formed can be determined. STAR claims that the Λ polarization, $\overline{\mathcal{P}}_{\Lambda}$, is parallel to the angular momentum $\hat{J}_{sys}$ of the QGP everywhere so that the vorticity $\omega = k_B T(\overline{\mathcal{P}}_{\Lambda} + \overline{\mathcal{P}}_{\overline{\Lambda}})/\hbar$ can be calculated, a good exercise for the reader to see if you can get the $\omega \sim 10^{22}/s$ which is 10^5 times larger than any other fluid [2]. Another interesting thing to note is that the largest vorticity is at

$\sqrt{s_{NN}} = 7.6 - 19$ GeV where the CERN fixed target experiments measure. Does this mean that their fluid (with minimal if any QGP) is also perfect?

STAR team receives secretary's achievement award for vorticity in 2018 (Figure 22).

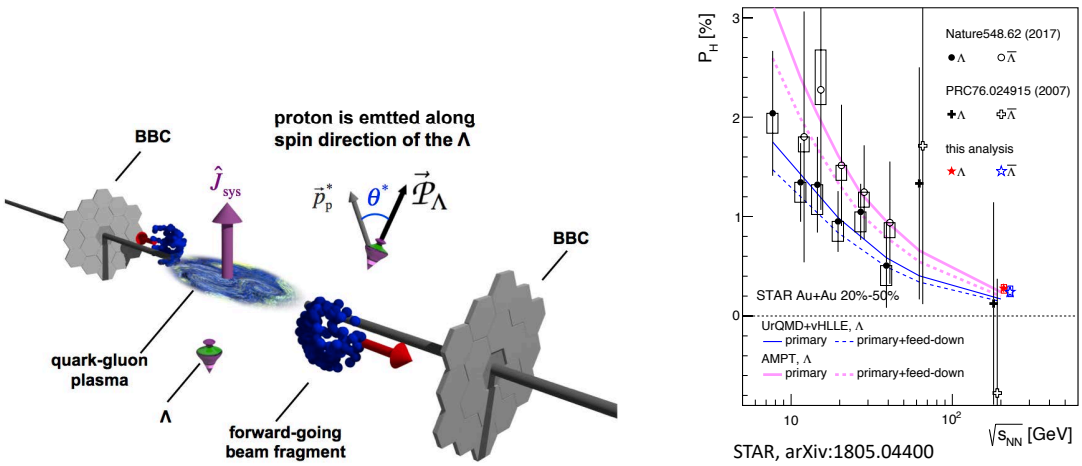

a) b)

Figure 21. (**a**) Schematic of STAR vorticity detection; and (**b**) polarization $P_H = \overline{\mathcal{P}}_\Lambda$ or $\overline{\mathcal{P}}_{\overline{\Lambda}}$ vs. $\sqrt{s_{NN}}$ [3].

STAR Team Receives Secretary's Achievement Award

Recognition for role in enabling discovery of fastest swirling matter at U.S. Departmer of Energy Office of Science user facility for nuclear physics research

+ENLARGE Members of the STAR team at the awards ceremony (l to r): William Christie, Zhangbu Xu, Victor Perevoztchikov, Dmitry Arkhipkin, Paul Sorensen, Energy Secretary Rick Perry, Jerome Lauret, James Dunlop, Gene Van Buren, Rachel Nieves, Flemming Videbaek, Robert Scheetz, Michael Poat, Dmitri Smirnov. Not shown: Elke-Caroline Aschenauer, Wayne Betts, Leslie Bland, Timothy Camarda, Zilong Chang, Lidia Didenko, Oleg Eyser, Salvatore Fazio, Yuri Fisyak, Wlodek Guryn, Levente Hajdu, John Hammond, Jiangyong Jia, Hongwei Ke, Alexander Kiselev, Jeffery Landgraf, Alexei Lebedev, Jeong-Hun Lee, Tonko Ljubic Rongrong Ma, Liz Mogavero, Akio Ogawa, Brian Page, Robert Pak, Lijuan Ruan, John Scheblein, Bill Schmidke, Rahul Sharma,

Figure 22. STAR receives an award for vorticity in 2018.

4. The Search for the Quark Gluon Plasma at RHIC

High energy nucleus–nucleus collisions provide the means of creating nuclear matter in conditions of extreme temperature and density, the Quark Gluon Plasma QGP (Figure 23). At large energy or baryon density, a phase transition is expected from a state of nucleons containing confined quarks and gluons to a state of "deconfined" (from their individual nucleons) quarks and gluons covering a volume that is many units of the confinement length.

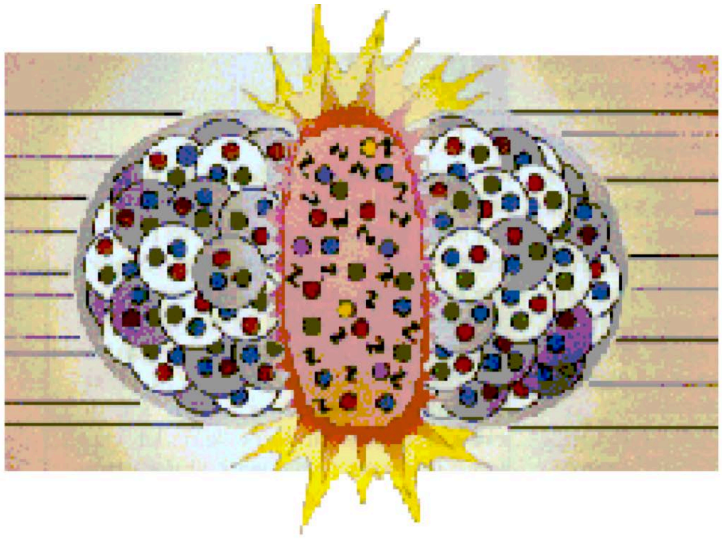

Figure 23. Sketch of nucleus–nucleus collision producing a QGP.

4.1. Anisotropic (Elliptical) Transverse Flow—An Interesting Complication in all A+A Collisions (Figure 24)

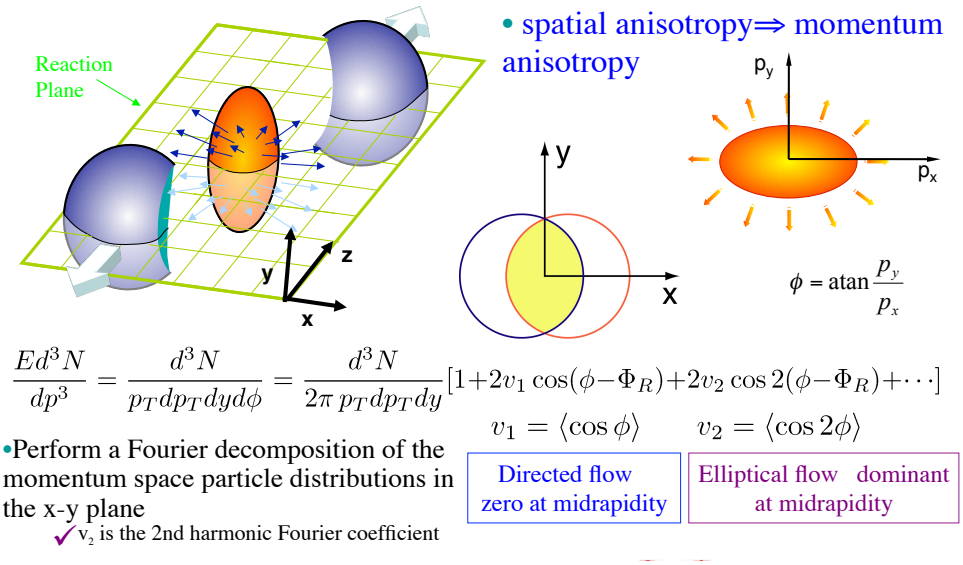

Figure 24. Sketch and definitions of elliptical flow, v_2.

Figure 25 shows that Elliptical flow (v_2) exists in all A+A collisions measured. At very low $\sqrt{s_{NN}}$, the main effect is from nuclei bouncing off each other and breaking into fragments. The negative v_2 at larger $\sqrt{s_{NN}}$ is produced by the effective "squeeze-out" (in the y direction) of the produced particles by slow moving minimally Lorentz-contracted spectators, which block the particles emitted in the reaction plane. With increasing $\sqrt{s_{NN}}$, the spectators move faster and become more contracted so the blocking stops and positive v_2 returns.

4.2. Flow Also Exists in Small Systems and Is Sensitive to the Initial Geometry

Figure 26 shows that flow exists in small p+Au, d+Au, ^{3}He+Au systems with preliminary sensitivity of v_3 to the initial geometry. Figure 27 (Top) shows that v_2 is about the same in all three systems

but v_3 is much larger in ^{3}He+Au, clearly indicating the sensitivity of flow to the initial geometry of the collision. Figure 27 (Bottom) shows that there is mass ordering in the flow which is strong evidence for hydrodynamics in these small systems. The solid red and dashed blue lines represent hydrodynamic predictions. These hydrodynamical models, which include the formation of a short-lived QGP droplet, provide the best simultaneous description of the measurements, strong evidence for the QGP in small systems.

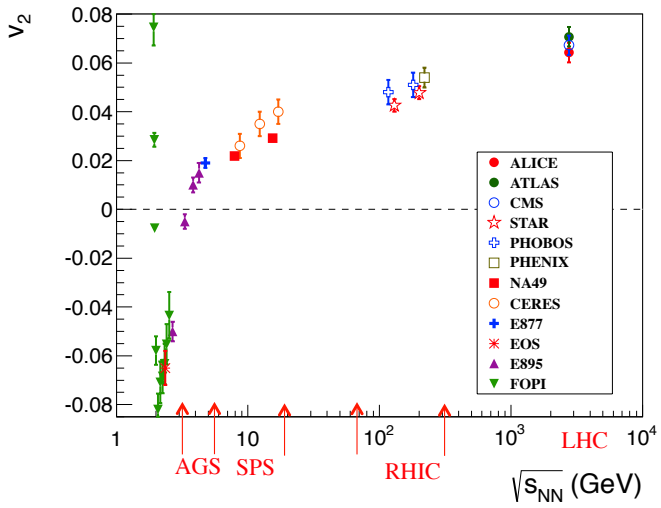

Figure 25. Values of elliptical flow (v_2) as a function of $\sqrt{s_{NN}}$ from all A+A collision measurements.

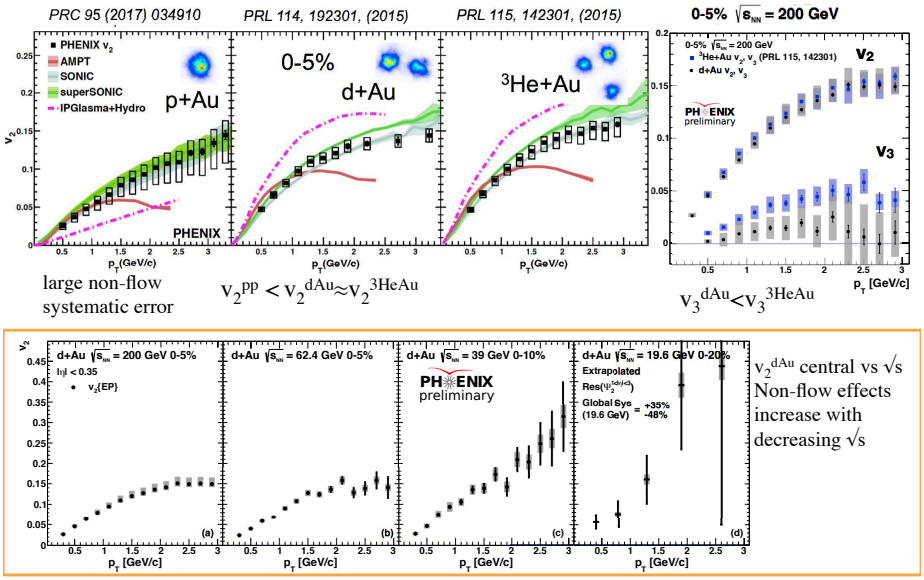

Figure 26. (**Top**) Published PHENIX v_2 measurements in p+Au, and 0-5% central d+Au and ^{3}He+Au collisions at $\sqrt{s_{NN}}$ =200 GeV, with preliminary v_2 and v_3 for the d+Au and ^{3}He+Au compared on the right. (**Bottom**) PHENIX preliminary v_2 in d+Au collisions as a function of $\sqrt{s_{NN}}$ with the centrality indicated illustrating that non-flow effects increase with decreasing $\sqrt{s_{NN}}$.

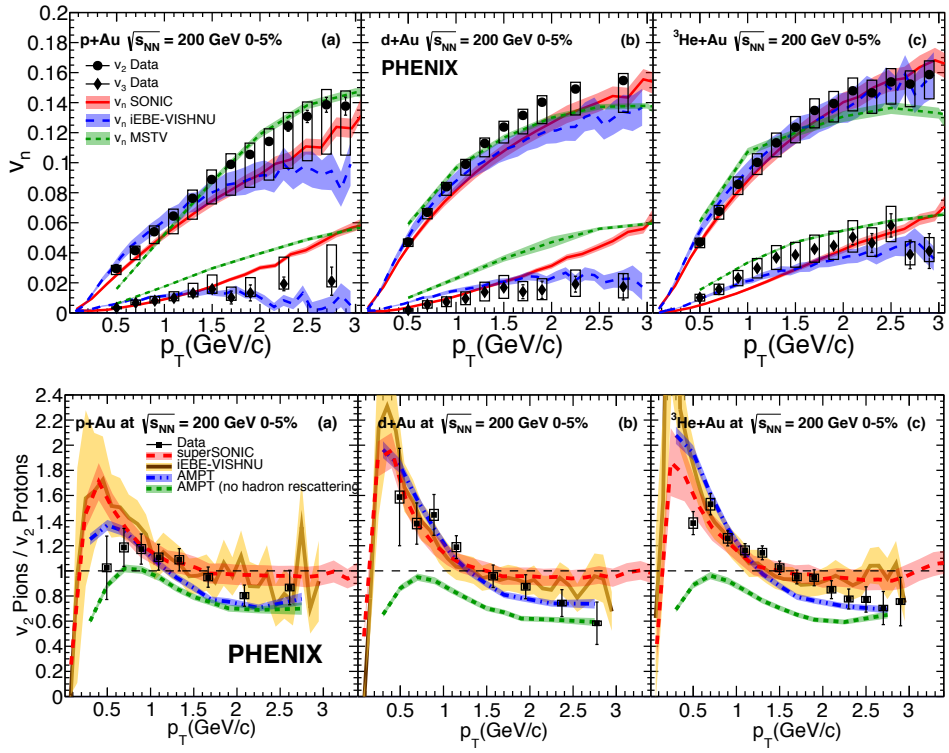

Figure 27. (**Top**) v_2 and v_3 in in 0–5% central (a) p+Au, (b) d+Au, (c) ^{3}He+Au collisions at $\sqrt{s_{NN}}$ = 200 GeV [4]. (**Bottom**) v_2 Pions/v_2 Protons in 0–5% central (a) p+Au, (b) d+Au, (c) ^{3}He+Au collisions at $\sqrt{s_{NN}}$ = 200 GeV [5].

4.2.1. It Takes Two Color Strings for Collectivity—Nagle, J.; et al. [6]

This is an answer to the interesting question of the minimal conditions for collectivity in small systems. For the case of e^+e^- collisions in Figure 28 utilizing the AAMPT framework and a single color string, the results indicate only a modest number of parton–parton scatterings and no observable collectivity signal.

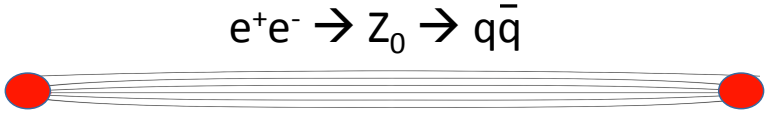

Figure 28. A fundamental point about QCD and the string tension between the q and $\bar{q}$.

However, a simple extension to two color strings (Figure 29), which represent a simplified geometry in p+p collisions, predicts finite long-range two-particle correlations (known as the ridge) and a strong v_2 with respect to the initial parton geometry.

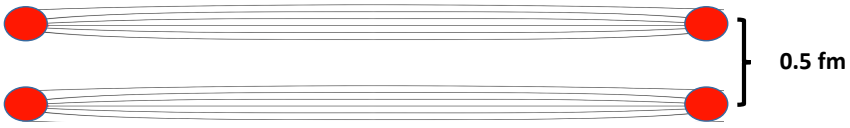

Figure 29. Additional special case—two Strings.

4.2.2. A Fundamental Point about QCD and the String Tension

Unlike an electric or magnetic field between two sources which spreads over all space, in QCD as proposed by Kogut and Susskind [7] the color flux lines connecting two quarks or a $q - \bar{q}$ pair as in Figure 28 are constrained in a thin tube-like region because of the three-gluon coupling. Furthermore, if the field contained a constant amount of color-field energy stored per unit length, this would provide a linearly rising confining potential between the $q - q$ or $q - \bar{q}$ pair.

This led to the Cornell string-like confining potential [8], which combined the Coulomb $1/r$ dependence at short distances from vector-gluon exchange with QCD coupling constant $\alpha_s(Q^2)$, and a linearly rising string-like potential, with string-tension σ,

$$V(r) = -\frac{\alpha_s}{r} + \sigma r \tag{1}$$

which provided confinement at large distances (Equation (1)). Particles are produced by the string breaking (fragmentation) .

4.3. The Latest Discovery Claims "Flow" in Small Systems Is From the QGP How Did We Find the QGP in the First Place?

4.3.1. J/ψ Suppression, 1986

In 1986, T. Matsui and H. Satz [9] said that due to the Debye screening of the color potential in a QGP, charmonium production would be suppressed since the c-$\bar{c}$ could not bind. With increasing temperature, T, in analogy to increasing Q^2, the strong coupling constant $\alpha_s(T)$ becomes smaller, reducing the binding energy, and the string tension, $\sigma(T)$, becomes smaller, increasing the confining radius, effectively screening the potential [10]

$$V(r) = -\frac{4}{3}\frac{\alpha_s}{r} + \sigma r \rightarrow -\frac{4}{3}\frac{\alpha_s}{r}e^{-\mu_D r} + \sigma\frac{(1 - e^{-\mu_D r})}{\mu_D} \tag{2}$$

where $\mu_D = \mu_D(T) = 1/r_D$ is the Debye screening mass. For $r < 1/\mu_D$, a quark feels the full color charge, but, for $r > 1/\mu_D$, the quark is free of the potential and the string tension, effectively deconfined. The properties of the QGP cannot be calculated in QCD perturbation theory but only in Lattice QCD Calculations [11].

J/ψ suppression eventually didn't work because the free c and $\bar{c}$ quarks recombined to make J/ψ's [12]. See Alice publication [13].

4.3.2. Jet Quenching by Coherent LPM Radiative Energy Loss of a Parton in the QGP, 1997

In 1997, Baier, Dokshitzer, Mueller, Peigne, Schiff and Zakharov (BDMPSZ) [14] said that the energy loss from coherent Landau–Pomeranchuk–Migdal (LPM) radiation for hard-scattered partons exiting the QGP would result in an attenuation of the jet energy and a broadening of the jets (Figure 30).

As a parton from hard-scattering in the A+B collision exits through the medium, it can radiate a gluon; and both continue traversing the medium. It is important to understand that "Only the gluons radiated outside the cone defining the jet contribute to the energy loss". In the angular ordering of QCD [15], the angular cone of any further emission will be restricted to be less than that of the previous emission and will end the energy loss once inside the jet cone. This does not work in the QGP so no energy loss occurs only when all gluons emitted by a parton are inside the jet cone. In addition to other issues, this means that defining the jet cone is a big issue—so watch out for so-called trimming.

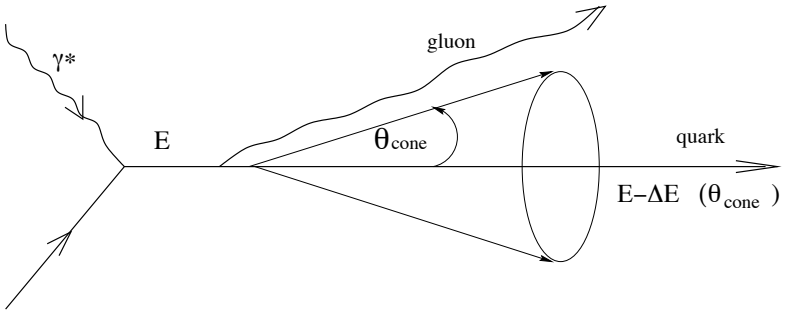

Figure 30. Jet Cone of an outgoing parton with energy E [14].

4.4. BDMPSZ: The Cone, the Energy Loss, Azimuthal Broadening, Is the QGP Signature

The energy loss of the outgoing parton, $-dE/dx$, per unit length (x) of a medium with total length L, is proportional to the total four-momentum transfer-squared, $q^2(L)$, and takes the form:

$$\frac{-dE}{dx} \simeq \alpha_s \langle q^2(L) \rangle = \alpha_s \, \mu^2 \, L/\lambda_{\rm mfp} = \alpha_s \, \hat{q} \, L$$

where μ, is the mean momentum transfer per collision, and the transport coefficient $\hat{q} = \mu^2/\lambda_{\rm mfp}$ is the four-momentum-transfer-squared to the medium per mean free path, $\lambda_{\rm mfp}$.

Additionally, the accumulated momentum-squared, $\langle p^2_{\perp W} \rangle$ transverse to a parton traversing a length L in the medium is well approximated by

$$\left\langle p^2_{\perp W} \right\rangle \approx \langle q^2(L) \rangle = \hat{q} L \qquad .$$

5. Jet Quenching at RHIC, the Discovery of the QGP

The energy loss of an outgoing parton with color charged fully exposed in a medium with a large density of similarly exposed color charges (i.e., a QGP) from Landau–Pomeranchuk–Migdal (LPM) coherent radiation of gluons was predicted in QCD by BDMPSZ [14].

Hard scattered partons (Figure 31a) lose energy going through the medium so that there are fewer partons or jet fragments at a given p_T. The ratio of the measured semi-inclusive yield of, for example, pions in a given A+A centrality class divided by the semi-inclusive yield in a p+p collision times the number of A+A collisions $\langle N_{\rm coll} \rangle$ in the centrality-class is given by the nuclear modification factor, R_{AA} (Figure 31b), which equals 1 for no energy loss.

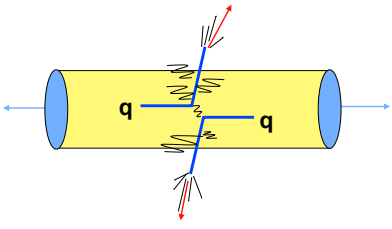

a)

b) $$R_{AA}(p_T) = \frac{d^2 N^{\pi}_{AA} \,/\, p_T dp_T dy N^{inel}_{AA}}{\left\langle N_{coll_{AA}} \right\rangle d^2 N^{\pi}_{pp} \,/\, p_T dp_T dy N^{inel}_{pp}}$$

Figure 31. (**a**) Hard quark–quark scattering in an A+A collision with the scattered quarks passing through the medium formed in the collision; and (**b**) nuclear modification factor $R_{AA}(p_T)$.

PHENIX discovered jet quenching of hadrons at RHIC in 2001 [16] (Figure 32). Pions at large $p_T > 2$ GeV/c are suppressed in Au+Au at $\sqrt{s_{NN}}$ =130 GeV compared to the enhancement found at the CERN SpS at $\sqrt{s_{NN}}$ =17 GeV. This is the first regular publication from a RHIC experiment to reach 1000 citations.

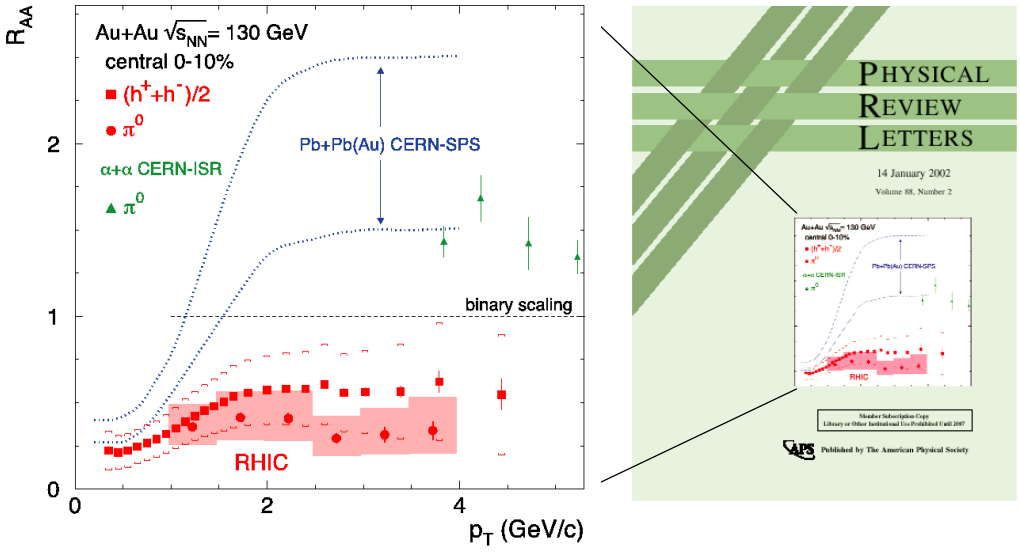

Figure 32. (**left**) Hadron suppression R_{AA} in Au+Au at $\sqrt{s_{NN}}$ = 130 GeV by PHENIX at RHIC compared to enhancement at $\sqrt{s_{NN}}$ = 17 GeV in Pb+Pb at the CERN SpS; and (**right**) plot is from the cover of PRL [16].

5.1. Status of R_{AA} in Au+Au at $\sqrt{s_{NN}}$ = 200 GeV

Figure 33 shows the suppression of all identified hadrons, as well as $e^{\pm}$ from c and b quark decay, with $p_T > 2$ GeV/c measured by PHENIX until 2013. One exception is the enhancement of protons for $2 < p_T < 4$ GeV/c, which are then suppressed at larger p_T. Particle Identification is crucial for these measurements since all particles behave differently. The only particle that shows no-suppression is the direct single γ (from the QCD reaction $g + q \rightarrow \gamma + q$) which shows that the medium produced at RHIC is the strongly interacting QGP since γ rays only interact electromagnetically.

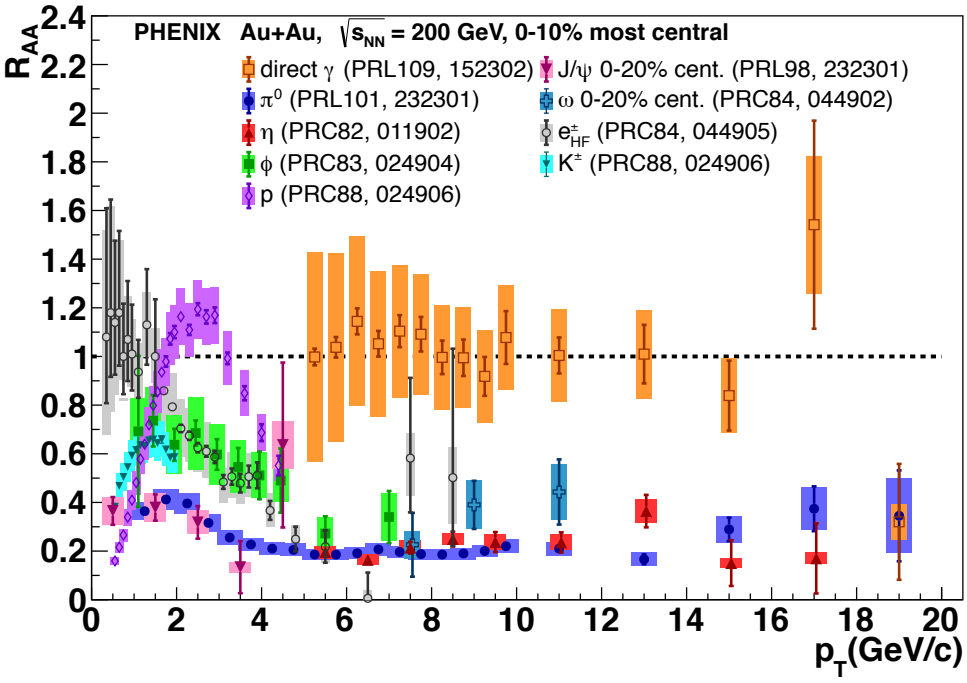

Figure 33. Published PHENIX measurements of R_{AA} with references.

5.2. Recent Measurements to Test the Second BDMPSZ Prediction

(1) The energy loss of the outgoing parton, $-dE/dx$, per unit length (x) of a medium with total length L, is proportional to the total four-momentum transfer-squared, $q^2(L)$, and takes the form:

$$\frac{-dE}{dx} \simeq \alpha_s \langle q^2(L) \rangle = \alpha_s \, \mu^2 \, L/\lambda_{\rm mfp} = \alpha_s \, \hat{q} \, L$$

where μ, is the mean momentum transfer per collision, and the transport coefficient $\hat{q} = \mu^2/\lambda_{\rm mfp}$ is the four-momentum-transfer-squared to the medium per mean free path, $\lambda_{\rm mfp}$.

(2) Additionally, the accumulated momentum-squared, $\langle p^2_{\perp W} \rangle$ transverse to a parton traversing a length L in the medium is well approximated by

$$\left\langle p^2_{\perp W} \right\rangle \approx \langle q^2(L) \rangle = \hat{q} \, L \qquad \langle \hat{q} L \rangle = \left\langle k^2_T \right\rangle_{AA} - \left\langle k'^2_T \right\rangle_{pp}. \tag{3}$$

Although only the component of $\langle p^2_{\perp W} \rangle \perp$ to the scattering plane affects k_T (Figure 34), the azimuthal broadening of the di-jet is caused by the random sum of the azimuthal components $\langle p^2_{\perp W} \rangle /2$ from each outgoing di-jet or $\langle p^2_{\perp W} \rangle = \hat{q} \, L$.

From the values of R_{AA} observed at RHIC (after 12 years), the JET Collaboration [17] has found that $\hat{q} = 1.2 \pm 0.3$ GeV^2/fm at RHIC, 1.9 ± 0.6 at LHC at an initial time $\tau_0 = 0.6$ fm/c; however, nobody has yet measured the azimuthal broadening predicted. Before proceeding, one has to know the meaning of k_T defined by Feynman, Field and Fox [18] as the transverse momentum of a parton in a nucleon (Figure 34).

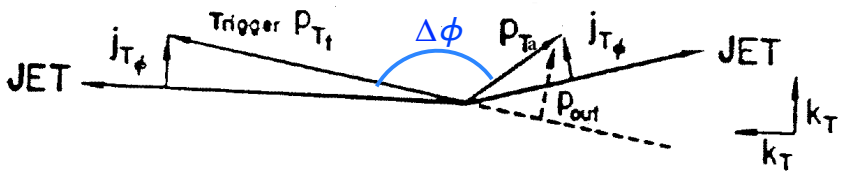

Figure 34. Sketch of a di-jet looking down the beam axis. The k_T from the two jets add randomly and are shown with one k_T perpendicular to the scattering plane, which makes the jets acoplanar in azimuth, and the other k_T parallel to the trigger jet, which makes the jets unequal in energy. in addition, $x_E = p_{Ta}\cos(\pi - \Delta\phi)/p_{Tt}$. The formula for calculating k_T from di-hadron correlations is given in Ref. [19].

5.2.1. The Key New Idea of $\left\langle k'^2_T \right\rangle_{pp}$ Instead of $\left\langle k^2_T \right\rangle_{pp}$ in Equation (3)

The di-hadron correlations of p_{Ta} with p_{Tt} (Figure 34) are measured in p+p and Au+Au collisions. The parent jets in the original Au+Au collision as measured in p+p will both lose energy passing through the medium but the azimuthal angle between the jets should not change unless the medium induces multiple scattering from $\hat{q}$. Thus, the calculation of k'_T from the di-hadron p+p measurement to compare with Au+Au measurements with the same di-hadron p_{Tt} and p_{Ta} must use the value of $\hat{x}_h$ and $\langle z_t \rangle$ of the parent jets in the A+A collision. The variables are $x_h \equiv p_{Ta}/p_{Tt}$, $\hat{x}_h \equiv \hat{p}_{Ta}/\hat{p}_{Tt}$, $\langle z_t \rangle \equiv p_{Tt}/\hat{p}_{Tt}$, where, e.g., p_{Tt} is the trigger particle transverse momentum and $\hat{p}_{Tt}$ means the trigger jet transverse momentum.

The same values of $\hat{x}_h$ and $\langle z_t \rangle$ in Au+Au and p+p give the cool result [20]:

$$\langle \hat{q}L \rangle = \left[\frac{\hat{x}_h}{\langle z_t \rangle}\right]^2 \left[\frac{\langle p^2_{\rm out}\rangle_{AA} - \langle p^2_{\rm out}\rangle_{pp}}{x^2_h}\right] \tag{4}$$

For di-jet measurements, the formula is even simpler:

(i) $x_h \equiv \hat{x}_h$ because the trigger and away "particles" are the jets; (ii) $\langle z_t \rangle \equiv 1$ because the trigger "particle" is the entire jet not a fragment of the jet; and (iii) $\langle p^2_{\rm out}\rangle = \hat{p}^2_{Ta}\sin^2(\pi - \Delta\phi)$. This reduces the formula for di-jets to:

$$\langle \hat{q}L \rangle = \left[\left\langle p^2_{\rm out}\right\rangle_{AA} - \left\langle p^2_{\rm out}\right\rangle_{pp}\right] = \hat{p}^2_{Ta}\left[\left\langle \sin^2(\pi - \Delta\phi)\right\rangle_{AA} - \left\langle \sin^2(\pi - \Delta\phi)\right\rangle_{pp}\right] \tag{5}$$

5.2.2. A Test of Equation (5) for $\langle \hat{q}L \rangle$

Al Mueller et al. [21] gave a prediction for the azimuthal broadening of di-jet angular correlations for 35 GeV jets at RHIC (Figure 35).

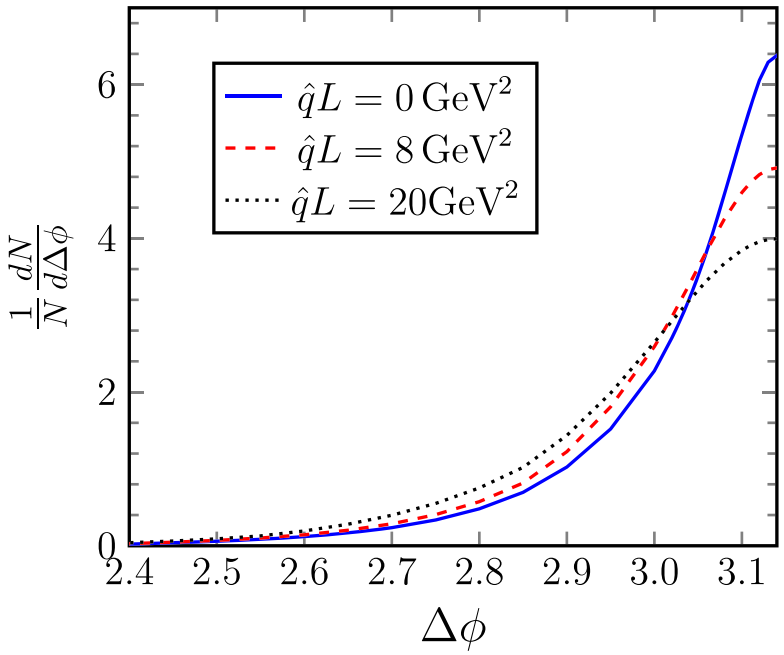

Figure 35. Prediction of folded away azimuthal width of 35 GeV/c Jets at RHIC for several values of $\hat{q}L$.

To check my Equation (5), I measured the half width at half maximum (HWHM), which equals 1.175σ for a Gaussian, for each curve in Figure 35, and calculated $(\sigma \times 35)^2$ to get $\langle p_{\mathrm{out}}^2 \rangle$ for each $\hat{q}L$, and used Equation (5) to get 9.6 GeV^2 and 21.5 GeV^2, respectively, for the 8 GeV^2 and 20 GeV^2 plots. This is an excellent result considering that I had to measure the HWHMs in Figure 35 with a pencil and ruler.

5.2.3. How to Calculate $\hat{q}L$ with Equation (4) from Di-Hadron Measurements

The determination of the required quantities is well known to older PHENIXians who have read Ref. [19] or my book [22] as outlined below:

(A) $\langle z_t \rangle$ is calculated from the Bjorken parent–child relation and "trigger bias" [23] (cf. Ref. [24]).

(B) The energy loss of the trigger jet from p+p to Au+Au can be measured by the shift in the p_T spectra [25].

(C) $\hat{x}_h$, the ratio of the away-jet to the trigger jet transverse momenta can be measured by the away particle p_{Ta} distribution for a given trigger particle p_{Tt} taking $x_E = x_h \cos\Delta\phi \approx x_h = p_{Ta}/p_{Tt}$ [19]:

$$\left.\frac{dP_\pi}{dx_E}\right|_{p_{T_t}} = N\,(n-1)\,\frac{1}{\hat{x}_h}\,\frac{1}{(1+\frac{x_E}{\hat{x}_h})^n} \quad . \tag{6}$$

5.2.4. Example: $\hat{x}_h$ from Fits to the PHENIX Data from Ref. [26]

The fits in Figure 36 work very well, with excellent χ^2/dof. However, it is important to notice that the dashed curve in Au+Au does not fit the data as well as the solid red curve which is the sum of Equation (6) with free parameters + a second term with the form of Equation (6) but with the $\hat{x}_h$ fixed at the p+p value. It is also important to note that the solid red curve between the highest Au+Au data points is notably parallel to the p+p curve. A possible explanation is that, in this region, which is at a fraction $\approx 1\%$ of the dP/dx_E distribution, the highest p_{Ta} fragments are from jets that do not lose energy in the QGP .

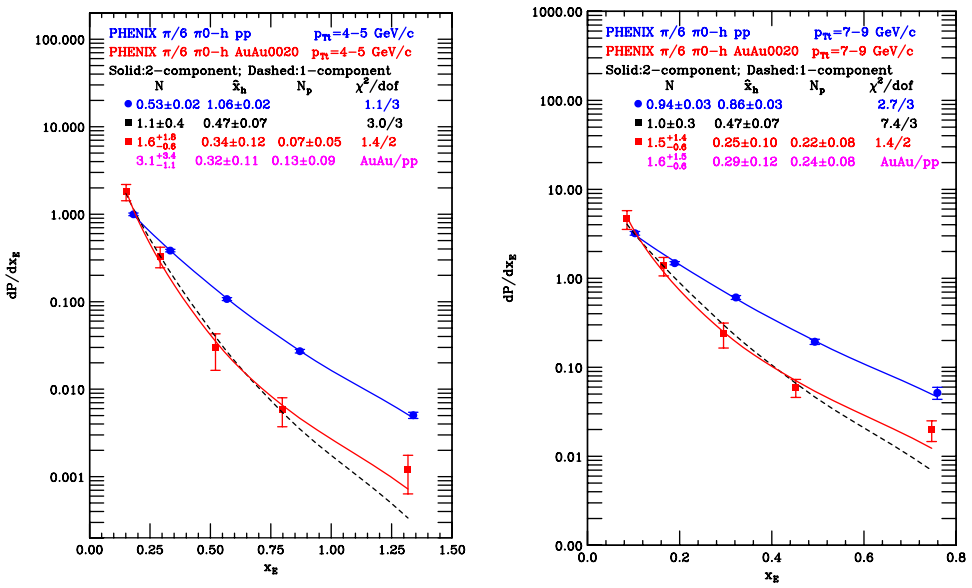

Figure 36. It to x_E distributions for $\pi^0 - h$ correlation in p+p and Au+Au 0–20% central collisions using Equation (6) with the results indicated: (**left**) $4 < p_{Tt} < 5$ GeV/c; and (**right**) $7 < p_{Tt} < 9$ GeV/c.

5.2.5. Results from STAR $\pi^0 - h$ and $\gamma - h$ Correlations [27]

Figure 37 is a table of results of my published calculation [20] of $\langle \hat{q}L \rangle$ from the STAR data. The errors on the STAR $\langle \hat{q}L \rangle$ here (with the *) are much larger than stated in my published calculation because I made a trivial mistake, which is corrected here. In addition, the new values of $\langle \hat{q}L \rangle$ reflect that Equation (4) defines $\langle \hat{q}L \rangle$ not $\langle \hat{q}L \rangle$ /2.

STAR PLB771						
$\sqrt{s_{NN}} = 200$	$\langle p_{Tt} \rangle$	$\langle p_{Ta} \rangle$	$\langle z_t \rangle$	$\hat{x}_h$	$\langle p^2_{\rm out} \rangle$	$\sqrt{\langle k^2_T \rangle}$
Reaction	GeV/c	GeV/c		GeV/c		GeV/c
p+p	14.71	1.72	0.80 ± 0.05	0.84 ± 0.04	0.263 ± 0.113	2.34 ± 0.34
p+p	14.71	3.75	0.80 ± 0.05	0.84 ± 0.04	0.576 ± 0.167	2.51 ± 0.31
Au+Au 00-12%	14.71	1.72	0.80 ± 0.05	0.36 ± 0.05	0.547 ± 0.163	2.28 ± 0.35
Au+Au 00-12%	14.71	3.75	0.80 ± 0.05	0.36 ± 0.05	0.851 ± 0.203	1.42 ± 0.22
p+p comp	14.71	1.72	0.80 ± 0.05	0.36 ± 0.05	0.263 ± 0.113	1.006 ± 0.18
p+p comp	14.71	3.75	0.80 ± 0.05	0.36 ± 0.05	0.576 ± 0.167	1.076 ± 0.18
						$\langle \hat{q}L \rangle$ GeV^2
Au+Au 00-12%	14.71	1.72				4.21 ± 3.24*
Au+Au 00-12%	14.71	3.75				0.86 ± 0.87*

Figure 37. $\hat{q}L$ result table for STAR $\pi^0 - h$, $12 < p_{Tt} < 20$ GeV/c 0-20% centrality.

5.3. Some $\langle \hat{q}L \rangle$ Results from PHENIX [26]

The away widths from PHENIX $\pi^0 - h$ correlations [26] are shown in Figure 38 with the calculated $\hat{q}L$ values for $\pi^0 - h$ $\sqrt{s_{NN}}$ = 200 GeV, 20–60% centrality, $5 < p_{Tt} < 7$ GeV/c shown in Figure 39 and $7 < p_{Tt} < 9$ GeV/c in Figure 40.

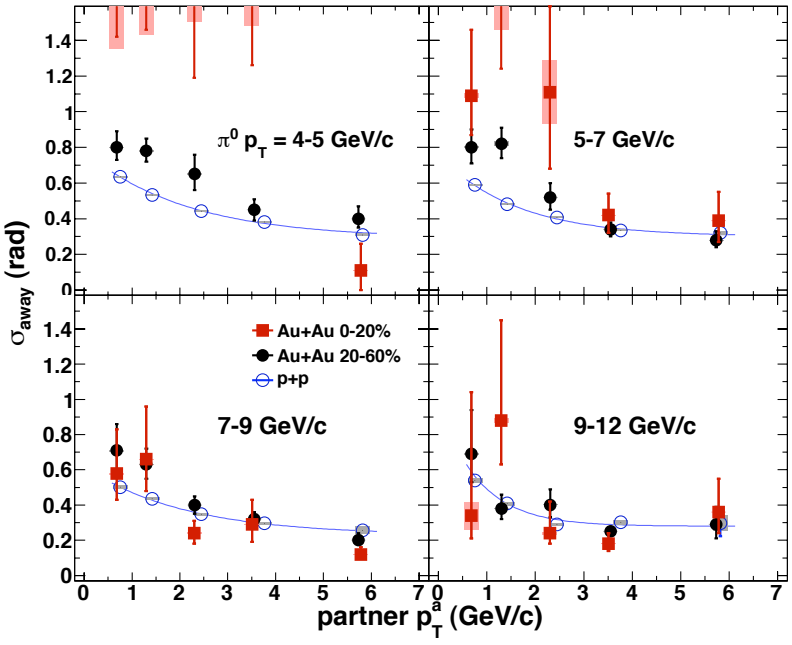

Figure 38. Away widths from $\pi^0 - h$ correlations as function of partner p_T, i.e., p_{Ta}, in Au+Au 0–20% and 20–60% and p+p collisions at $\sqrt{s_{NN}}$ = 200 GeV for four ranges of trigger p_{Tt} indicated [26].

PHENIX PRL104						
$\sqrt{s_{NN}} = 200$	$\langle p_{Tt}\rangle$	$\langle p_{Ta}\rangle$	$\langle z_t\rangle$	$\hat{x}_h$	$\langle p^2_{\rm out}\rangle$	$\sqrt{\langle k^2_T\rangle}$
Reaction	GeV/c	GeV/c		GeV/c		GeV/c
p+p	5.78	1.42	0.60 ± 0.06	0.96 ± 0.02	0.434 ± 0.010	3.13 ± 0.37
p+p	5.78	2.44	0.60 ± 0.06	0.96 ± 0.02	0.934 ± 0.031	3.18 ± 0.34
p+p	5.78	3.76	0.60 ± 0.06	0.96 ± 0.02	1.523 ± 0.061	2.74 ± 0.29
p+p	5.78	5.82	0.60 ± 0.06	0.96 ± 0.02	3.339 ± 0.351	2.73 ± 0.32
Au+Au 20-60%	5.78	1.30	0.62 ± 0.06	0.69 ± 0.05	0.867 ± 0.116	4.04 ± 0.61
Au+Au 20-60%	5.78	2.31	0.62 ± 0.06	0.69 ± 0.05	1.291 ± 0.308	2.88 ± 0.54
Au+Au 20-60%	5.78	3.55	0.62 ± 0.06	0.69 ± 0.05	1.370 ± 0.249	1.90 ± 0.32
Au+Au 20-60%	5.78	5.73	0.62 ± 0.06	0.69 ± 0.05	2.562 ± 0.620	1.66 ± 0.31
p+p comp	5.78	1.30	0.62 ± 0.06	0.69 ± 0.05	0.434 ± 0.010	2.39 ± 0.32
p+p comp	5.78	2.31	0.62 ± 0.06	0.69 ± 0.05	0.934 ± 0.031	2.34 ± 0.29
p+p comp	5.78	3.55	0.62 ± 0.06	0.69 ± 0.05	1.522 ± 0.061	2.03 ± 0.25
p+p comp	5.783	5.73	0.62 ± 0.06	0.69 ± 0.05	3.339 ± 0.351	1.93 ± 0.26
					$\langle \hat{q}L\rangle$ .01	$\langle \hat{q}L\rangle$ GeV^2
Au+Au 20-60%	5.78	1.30			6.9 ± 3.6	10.6 ± 3.8
Au+Au 20-60%	5.78	2.31			2.3 ± 2.1	2.8 ± 2.4
Au+Au 20-60%	5.78	3.55			0.35 ± 0.93	-0.5 ± 0.9
Au+Au 20-60%	5.78	5.73			-0.75 ± 1.0	-1.0 ± 0.9

Figure 39. $\hat{q}L$ result table for PHENIX $\pi^0 - h$, $5 < p_{Tt} < 7$ GeV/c 20–60% centrality.

PHENIX PRL104						
$\sqrt{s_{NN}} = 200$	$\langle p_{Tt} \rangle$	$\langle p_{Ta} \rangle$	$\langle z_t \rangle$	$\hat{x}_h$	$\langle p^2_{\rm out} \rangle$	$\sqrt{\langle k^2_T \rangle}$
Reaction	GeV/c	GeV/c		GeV/c		GeV/c
p+p	7.83	1.42	0.64 ± 0.06	0.86 ± 0.03	0.360 ± 0.017	2.98 ± 0.41
p+p	7.83	2.44	0.64 ± 0.06	0.86 ± 0.03	0.694 ± 0.048	2.99 ± 0.34
p+p	7.83	3.76	0.64 ± 0.06	0.86 ± 0.03	1.213 ± 0.109	2.76 ± 0.32
p+p	7.83	5.82	0.64 ± 0.06	0.86 ± 0.03	2.177 ± 0.424	2.48 ± 0.38
Au+Au 20-60%	7.83	1.30	0.66 ± 0.06	0.62 ± 0.04	0.548 ± 0.107	3.35 ± 0.64
Au+Au 20-60%	7.83	2.31	0.66 ± 0.06	0.62 ± 0.04	0.803 ± 0.177	2.45 ± 0.46
Au+Au 20-60%	7.83	3.55	0.66 ± 0.06	0.62 ± 0.04	1.237 ± 0.232	2.08 ± 0.34
Au+Au 20-60%	7.83	5.73	0.66 ± 0.06	0.62 ± 0.04	1.300 ± 0.350	1.29 ± 0.27
p+p comp	7.83	1.30	0.66 ± 0.06	0.62 ± 0.04	0.360 ± 0.017	2.28 ± 0.33
p+p comp	7.83	2.31	0.66 ± 0.06	0.62 ± 0.04	0.694 ± 0.048	2.22 ± 0.28
p+p comp	7.83	3.55	0.66 ± 0.06	0.62 ± 0.04	1.213 ± 0.109	2.05 ± 0.26
p+p comp	7.83	5.73	0.66 ± 0.06	0.62 ± 0.04	2.177 ± 0.424	1.76 ± 0.28
					$\langle \hat{q}L \rangle$ .01	$\langle \hat{q}L \rangle$ GeV^2
Au+Au 20-60%	7.83	1.30			9.3 ± 6.3	6.0 ± 3.7
Au+Au 20-60%	7.83	2.31			2.4 ± 2.2	1.1 ± 1.9
Au+Au 20-60%	7.83	3.55			1.0 ± 1.2	0.11 ± 1.1
Au+Au 20-60%	7.83	5.73			-1.2 ± 1.0	-1.4 ± 1.0

Figure 40. $\hat{q}L$ result table for PHENIX $\pi^0 - h$, $7 < p_{Tt} < 9$ GeV/c 20–60% centrality.

5.4. Conclusions

It appears that the method works and gives consistent results for all the $\hat{q}L$ calculations shown (Figures 37, 39 and 40). In the lowest $p_{Ta} \sim 1.5$ GeV/c bin, the results are all consistent with the JET collaboration [17] result, $\hat{q} = 1.2 \pm 0.3$ GeV^2/fm or $\hat{q}L = 8.4 \pm 2.1$ GeV^2 for $L = 7$ fm, the radius of an Au nucleus. However, for $p_{Ta} > 2.0$ GeV/c, all the results are consistent with $\hat{q}L = 0$. Personally, I think that this is where the first gluon emitted in the medium was inside the jet cone, so that all further emissions were also inside the jet cone due to the angular ordering of QCD so that there is no evident suppression; or that jets with fragments with $p_T \geq 3$ GeV/c, which are distributed narrowly about the jet axis, are not strongly affected by the medium [28]. I think that this also agrees with the observation in Figure 36 that two or three orders of magnitude down in the $x_E = p_{Ta}/p_{Tt}$ distributions the A+A best fit is parallel to the p+p measurement, which means that these A+A fragments are from jets that have not lost energy. This is consistent with all the $I_{AA} = x_E^{AA}/x_E^{pp} = (p_{Ta}^{AA}/p_{Ta}^{pp})|_{p_{Tt}}$ distributions ever measured (e.g., Figures 41 and 42), which decrease with increasing p_{Ta} until $p_{Ta} \approx 3$ GeV/c and then remain constant because the A+A and p+p distributions are parallel due to no jet energy loss for fragments in this range.

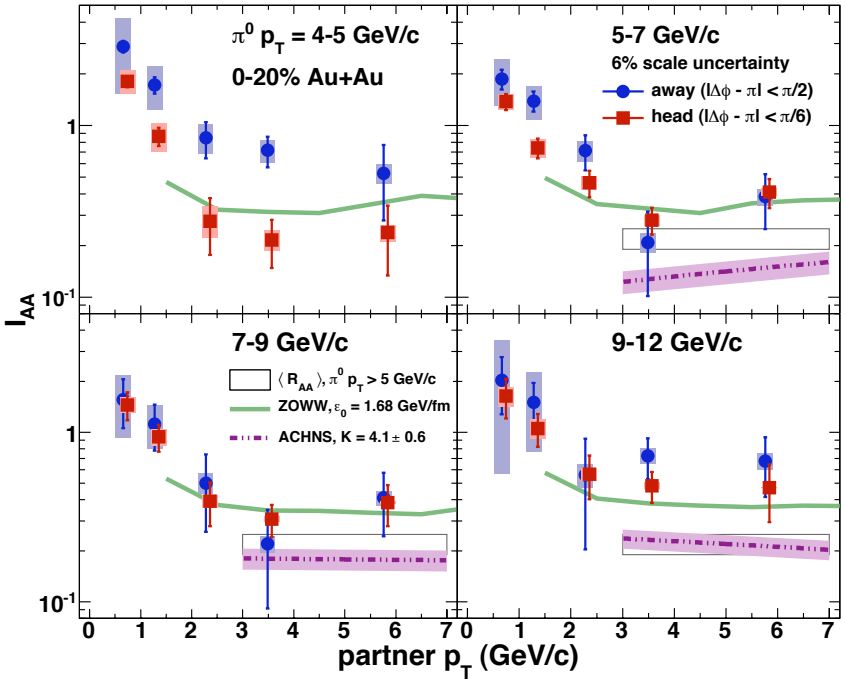

Figure 41. PHENIX I_{AA} distribution [26].

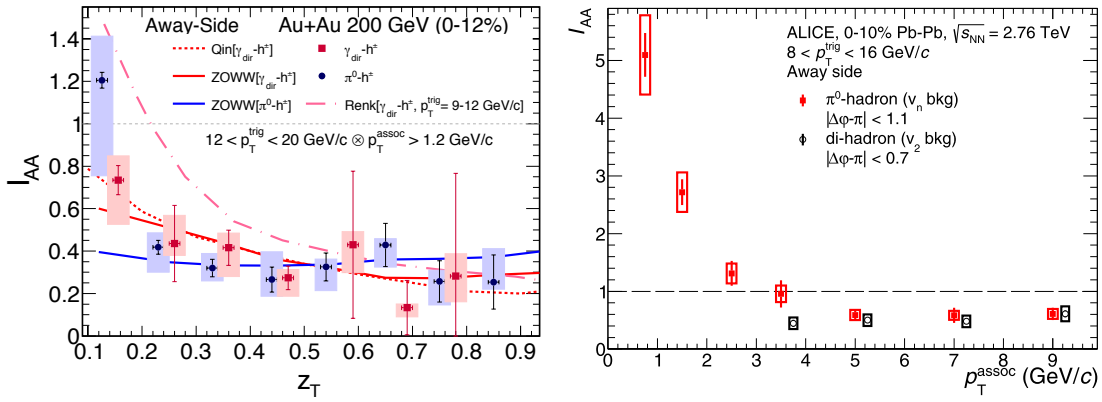

Figure 42. (**left**) STAR I_{AA} distribution [27]; and (**right**) ALICE I_{AA} distribution [29].

Funding: The research was supported by U. S. Department of Energy, DE-SC0012704.

Conflicts of Interest: The author declares no conflict of interest.

References

1. Bunce, G.; et al. [WMR Collaboration]. Λ^0 Hyperon Polarization in Inclusive Production by 300-GeV Protons on Beryllium. *Phys. Rev. Lett.* **1976**, *36*, 1113–1116. [CrossRef]
2. Adamczyk, L.; et al. [STAR Collaboration]. Global Λ hyperon polarization in nuclear collisions. *Nature* **2017**, *548*, 62–65.
3. Adam, J.; et al. [STAR Collaboration]. Global polarization of Λ hyperons in Au+Au collisions at $\sqrt{s_{NN}}$ = 200 GeV. *Phys. Rev. C* **2018**, *98*, 014910. [CrossRef]

4. Aidala, C.; et al. [PHENIX Collaboration]. Creation of quark-gluon plasma droplets with three distinct geometries. *Nat. Phy.* **2019**, *15*, 214–220.
5. Adare, A.; et al. [PHENIX Collaboration]. Measurements of mass-dependent azimuthal anisotropy in central p+Au, d+Au and ^{3}He+Au collisions at $\sqrt{s_{NN}}$ = 200 GeV. *Phys. Rev. C* **2018**, *97*, 064904. [CrossRef]
6. Nagle, J.L.; Belmont, R.; Hill, K.; Orjuela Koop, J.; Perepelitsa, D.V.; Yin, P.; Lin, Z.-W.; McGlinchey, D. Minimal conditions for collectivity in e^+e^- and $p+p$ collisions. *Phys. Rev. C* **2018**, *97*, 024909. [CrossRef]
7. Kogut, J.; Susskind, L. Vacuum polarization and the absence of free quarks in four dimensions. *Phys. Rev. D* **1974**, *9*, 3501–3512. [CrossRef]
8. Eichten, E.; Gottfried, K.; Kinoshita, T.; Kogut, J.; Lane, K.D.; Yan, T.-M. Spectrum of Charmed Quark-Antiquark Bound States. *Phys. Rev. Lett.* **1975**, *34*, 369–372. [CrossRef]
9. Matsui, T.; Satz, H. J/ψ Suppression by Quark-Gluon Plasma Formation. *Phys. Lett. B* **1987**, *178*, 416–422. [CrossRef]
10. Satz, H. Colour deconfinement in nuclear collisions. *Rep. Prog. Phys.* **2000**, *63*, 1511–1574. [CrossRef]
11. Soltz, R.A.; DeTar, C.; Karsch. F.; Mukherjee, S.; Vranas, P. Lattice QCD Thermodynamics with Physical Quark Masses. *Ann. Rev. Nucl. Part. Sci.* **2015**, *65*, 379. [CrossRef]
12. Braun-Munzinger, P.; Stachel, J. (Non) thermal aspects of charmonium production and a new look at J/ψ suppression. *Phys. Lett. B* **2000**, *490*, 196. [CrossRef]
13. Abelev, B.; et al. [ALICE Collaboration]. J/ψ Suppression at Forward Rapidity in Pb-Pb Collisions at $\sqrt{s_{NN}}$ = 2.76 TeV. *Phys. Rev. Lett.* **2012**, *109*, 072301. [CrossRef] [PubMed]
14. Baier, R.; Schiff, D.; Zakharov, B.G. Energy Loss in Perturbative QCD. *Ann. Rev. Nucl. Part. Sci.* **2000**, *50*, 37–69. [CrossRef]
15. Mueller, A.H. On the multiplicity of hadrons in QCD jets. *Phys. Lett. B* **1981**, *104*, 161–164. [CrossRef]
16. Adcox, K.; et al. [PHENIX Collaboration]. Suppression of Hadrons with Large Transverse Momentum in Central Au+Au Collisions at $\sqrt{s_{NN}}$ =130 GeV. *Phys. Rev. Lett.* **2002**, *88*, 022301. [CrossRef] [PubMed]
17. Burke, K.M.; et al. [JET Collaboration]. Extracting the jet transport coefficient from jet quenching in high-energy heavy-ion collisions. *Phys. Rev. C* **2014**, *90*, 014909. [CrossRef]
18. Feynman, R.P.; Field, R.D.; Fox, G.C. Correlations among particles and jets produced with large transverse momenta. *Nucl. Phys. B* **1977**, *128*, 1–65. [CrossRef]
19. Adler, S.S.; et al. [PHENIX Collaboration]. Jet properties from dihadron correlations in p+p collisions at $\sqrt{s}$ = 200 GeV. *Phys. Rev. D* **2006**, *74*, 072002. [CrossRef]
20. Tannenbaum, M. J. Measurement of $\hat{q}$ in Relativistic Heavy Ion Collisions using di-hadron correlations. *Phys. Lett. B* **2017**, *771*, 553–557. [CrossRef]
21. Mueller, A.H.; Wu, B.; Xiao, B.-W.; Yuan, F. Probing transverse momentum broadening in heavy ion collisions. *Phys. Lett. B* **2016**, *763*, 208–212. [CrossRef]
22. Rak, J.; Tannenbaum, M.J. *High p_T Physics in the Heavy Ion Era*; Cambridge University Press: Cambridge, UK, 2013; pp. 1–387.
23. Jacob, M.; Landshoff, P.V. Large Transverse Momentum and Jet Studies. *Phys. Repts.* **1978**, *48*, 285–350. [CrossRef]
24. Adare, A.; et al. [PHENIX Collaboration]. Double-helicity dependence of jet properties from dihadrons in longitudinally polarized p+p collisions at $\sqrt{s_{NN}}$ = 200 GeV. *Phys. Rev. D* **2010**, *81*, 012002. [CrossRef]
25. Adare, A.; et al. [PHENIX Collaboration]. Neutral pion production with respect to centrality and reaction plane in Au+Au collisions at $\sqrt{s_{NN}}$ = 200 GeV. *Phys. Rev. C* **2013**, *87*, 034911. [CrossRef]
26. Adare, A.; et al. [PHENIX Collaboration]. Transition in Yield and Azimuthal Shape Modification in Dihadron Correlations in Relativistic Heavy Ion Collisions. *Phys. Rev. Lett.* **2010**, *104*, 252301. [CrossRef] [PubMed]
27. Adamczyk, L.; et al. [STAR Collaboration]. Jet-like correlations with direct-photon and neutral-pion triggers at $\sqrt{s_{NN}}$ = 200 GeV. *Phys. Lett. B* **2016**, *760*, 689–696.[CrossRef]

28. Methar-Tani, Y.; Milhano, J.G.; Tywoniuk, K. Jets in Heavy-Ion Collisions. *Int. J. Mod. Phys. A* **2013**, *28*, 1340013. [CrossRef]
29. Adam, J.; et al. [ALICE Collaboration]. Jet-like correlations with neutral pion triggers in pp and central Pb-Pb collisions at 2.76 TeV. *Phys. Lett. B* **2016**, *763*, 238–250. [CrossRef]